

DEPARTMENT OF MATHEMATICS AND COMPUTING SCIENCES
SCHOOL OF SCIENCES AND HEALTH PROFESSIONS
OLD DOMINION UNIVERSITY
NORFOLK, VIRGINIA

A NUMERICAL INVESTIGATION OF THE FINITE ELEMENT
METHOD IN COMPRESSIBLE PRIMITIVE VARIABLE
NAVIER-STOKES FLOW

By

C. H. Cooke

(NASA-CR-153217) A NUMERICAL INVESTIGATION N77-24424
OF THE FINITE ELEMENT METHOD IN COMPRESSIBLE
PRIMITIVE VARIABLE NAVIER-STOKES FLOW Final
Report (Old Dominion Univ., Norfolk, Va.) Unclas
62 p HC A04/MF A01 CSCL 20D G3/34 30353

Final Report

Prepared for the
National Aeronautics and Space Administration
Langley Research Center
Hampton, Virginia 23665

Under
Grant NSG 1098
J. E. Harris, Technical Monitor
High Speed Aerodynamics Division

May 1977

REPRODUCED BY
NATIONAL TECHNICAL
INFORMATION SERVICE
U. S. DEPARTMENT OF COMMERCE
SPRINGFIELD, VA. 22161



DEPARTMENT OF MATHEMATICS AND COMPUTING SCIENCES
SCHOOL OF SCIENCES AND HEALTH PROFESSIONS
OLD DOMINION UNIVERSITY
NORFOLK, VIRGINIA

A NUMERICAL INVESTIGATION OF THE FINITE ELEMENT
METHOD IN COMPRESSIBLE PRIMITIVE VARIABLE
NAVIER-STOKES FLOW

By

C. H. Cooke

Final Report

Prepared for the

National Aeronautics and Space Administration
Langley Research Center
Hampton, Virginia 23665

Under

Grant NSG 1098
J. E. Harris, Technical Monitor
High Speed Aerodynamics Division

Submitted by the

Old Dominion University Research Foundation
Norfolk, Virginia 23508



May 1977

CONTENTS

| | Page |
|--|------|
| SUMMARY | 1 |
| INTRODUCTION | 2 |
| A CRITIQUE OF THE FINITE ELEMENT METHOD (FEM) | 4 |
| The Advantages of FEM | 5 |
| The Adverseness of Finite Elements in Fluid Dynamics | 7 |
| Relationship Between FEM and FDM Discretizations | 8 |
| The Linear Element Model | 8 |
| FEM Equations on a Nonuniform Grid | 9 |
| FEM Equations on Uniform Grid | 10 |
| Inconsistent FEM | 11 |
| Extra Stiffness of FEM Systems | 13 |
| Storage Considerations | 14 |
| Time Considerations | 16 |
| FINITE ELEMENT MODEL OF NOZZLE AFTERBODY VISCOUS INTERACTION EFFECTS WITH PLUME SIMULATION | 17 |
| The Navier-Stokes Equations | 18 |
| Cartesian Coordinates | 19 |
| Axis-symmetric Cylindrical Coordinates | 21 |
| The Galerkin FEM Equations | 22 |
| Boundary Conditions | 24 |
| NUMERICAL RESULTS | 25 |
| Oblique Shock Flow | 25 |
| Boattail Afterbody Flow with Separation | 27 |
| Comparisons of Computational Efficiency | 29 |
| CONCLUSIONS | 31 |
| APPENDIX I--A SPLIT BAND-CHOLESKY EQUATION-SOLVING STRATEGY FOR FINITE ELEMENT ANALYSIS OF TRANSIENT FIELD PROBLEMS | 47 |
| Abstract | 47 |
| Introduction | 47 |
| The Split-Cholesky Philosophy | 50 |
| Mesh Considerations | 51 |
| REFERENCES | 55 |

CONTENTS--Concluded

Page

LIST OF TABLES

| | |
|---|----|
| Table 1. Conditions for Oblique Shock Simulation. | 26 |
| Table 2. Comparison of FEM/FDM Performance Characteristics. | 30 |

LIST OF FIGURES

| | |
|--|----|
| Figure 1. Finite element irregular triangulated gridwork. | 34 |
| Figure 2. Boattail plume simulator flow field. | 35 |
| Figure 3. Oblique shock computational domain. | 36 |
| Figure 4. Boattail computational domain, with irregular triangular element formation. | 37 |
| Figure 5. Oblique shock FEM-FDM computational results (Re = 80,869). | 38 |
| Figure 6. Boattail afterbody FEM-FDM computational results (Re = 12,365). | 41 |
| Diagram One. The reduction of a band matrix. | 53 |
| Diagram Two. Mesh Processing Considerations. | 54 |

A NUMERICAL INVESTIGATION OF THE FINITE ELEMENT METHOD IN
COMPRESSIBLE PRIMITIVE VARIABLE NAVIER-STOKES FLOW

By

C. H. Cooke¹

SUMMARY

The results of a comprehensive numerical investigation of the basic capabilities of the finite element method (FEM) for numerical solution of compressible flow problems governed by the two-dimensional and axis-symmetric Navier-Stokes equations in primitive variables are presented. The strong and weak points of the method as a tool for computational fluid dynamics are considered. The relation of the linear element finite element method to finite difference methods (FDM) is explored.

The calculation of free shear layer and separated flows over aircraft boattail afterbodies with plume simulators indicate the strongest assets of the method are its capabilities for reliable and accurate calculation employing variable grids which readily approximate complex geometry and capably adapt to the presence of diverse regions of large solution gradients without the necessity of domain transformation. In all cases, numerical results have been in excellent agreement with those obtained by finite difference solution of the same physical problems, for diverse flows (some with embedded shocks) and a wide range of Reynolds numbers.

However, for sufficiently complex equations, finite element time marching schemes as presently conceived do not appear able to compete economically with the better finite difference methods of comparable accuracy. Greater overhead may be expected with the method in terms of both computer resources and man-year effort. The outstanding weakness of the finite element methodology

¹ Associate Professor of Mathematical and Computing Sciences, Old Dominion University, Norfolk, Virginia 23508.

is the amount of computer time required to produce acceptable problem solutions. The greatest future of the method in Navier-Stokes flows appears to be with the approach of seeking at the outset the solution of the steady state equations, where the high overhead per iterative step is offset by rapid convergence with a minimum of iterations.

INTRODUCTION

During the past three decades fluid dynamics in the aerospace industry has provided a major impetus to the development of methods for the numerical solution of partial differential equations. Finite difference methods (FDM) have been extensively investigated, to the point that the flexibility, versatility, and adequacy of the various FDM techniques have firmly established it as the leading method for the numerical modeling of complex fluid dynamic problems. Somewhat more recently studies have been directed to the investigation of the finite element method (FEM) as an alternative tool. The method is unquestionably well respected in the fields of structural and solid mechanics, where the dynamic interactions in complex configurations such as perhaps an aircraft wing frame with many easily identified component parts may be modeled by considering each structural member as an element of the finite element system, logically as well as physically connected at the nodes of the problem.

However, the modeling of a near inviscid fluid continuum by small subcontinua suitably joined at certain points, lines, or planes, does not appear as intuitively natural as does the near inelastic solid continuum model. Of perhaps greater significance is the general tendency to cumbersome experienced in the application of the FEM technique, which exhibits less flexibility towards individual innovation in general and in particular in the differencing of specific equation terms than is allowed by the customary FDM methods. Indeed, the general manner in which FEM computational results have been reported have led some to believe the method has been oversold. As Roache (ref. 1) phrases the call for a more exacting critique of the method, "Perhaps it is time for someone to comment on the emperor's new clothes."

Here we do not intend to imply that accurate computational results are difficult to achieve; this is the rule rather than the exception, and represents one of the major strong points of FEM. However, to quote Sabir (ref. 2): "While considerable attention has been given in the published literature to efficiency and speed of (linear system) solution routines, little or no attention is given to the total time taken by computers in producing acceptable solutions." Although the characteristics of the method have not been thoroughly assessed, it appears predictable that, aside from possibly potential flow calculations (ref. 3) or in some boundary layer problems (ref. 4), in general FEM results can only be obtained at excessive costs. The hindrance of associated time-consuming computer runs exorbitantly demanding of core storage, auxiliary devices, etc., is particularly hard to abide in batch-oriented computer systems fine tuned for rapid processing of myriad small jobs. Moreover, it does not seem that this deficiency will be remedied by the next generation of advanced computer technology, since the method is in many respects not highly vectorizable.

Perhaps more specifically, it does not appear that in their present conception the FEM time marching schemes for asymptotic calculation of steady high speed flows governed by the compressible Navier-Stokes equations in primitive variable form will ever be economically feasible, in comparison to the relatively greater economy provided by the better FDM methods, together with stretching transformations to simplify complex geometry. For problems whose simplification requires shearing as well as stretching in domain transformation, or for problems whose solution is sought at the outset by resort to the steady governing equations, the future of the method may not be as dark. It has been pointed out that the economic difficulties characteristic of the method are perhaps due in some respects to the tendency to the frontal attack on computational problems by FEM practitioners, as customary in the FDM approach. It may be that more success with the method in the future will result from taking another look at analytic methods such as quasi-linearization or local Prandtl-Glauert approximation (refs. 7, 8) together with iterating nonlinearities, which have in the past

not been considered feasible. Certainly for those cases in which the high overhead per iterative step is compensated by accelerated convergence rates requiring few computational steps to convergence the comparative economy of the method is yet to be decided (refs. 3 to 10). However, the FDM practitioners are making rapid progress in these areas as well (refs. 11, 12), and FDM could again overstride the FEM results--for the same reasons, the cumbersomeness of the approach. It could be there are special classes of problems such as in transonic flows (ref. 13) or large scale meteorological studies (refs. 6, 13, 14, 16) where FDM practice is not sufficiently advanced or the mathematical intricacies of the physical problem not well understood that FEM technology in the hands of an able practitioner will make a contribution. In general, these special cases are not too well known or as yet await recognition.

A CRITIQUE OF THE FINITE ELEMENT METHOD (FEM)

A comprehensive investigation of the FEM methods applied to compressible flows governed by the two-dimensional Navier-Stokes equations has been undertaken by the author. Four distinct primitive variable codes have been developed. Flow calculations are performed for several problem classes: free shear layer flows at $Re = 1000$, for fully supersonic ($M = 3$) and mixed subsonic-supersonic ($M = 1.68$ to $M = 3$) jet mixing; a uniform flow with embedded oblique shock but no recirculation, at $Re = 80$ and $Re = 80,000$; and the mixing and recirculating flow with weak shock (at $Re = 12,365$) represented by the boattail afterbody problem.

For the free shear layer flow problems in rectangular coordinates the constant total temperature assumption employed allowed the energy equation to be replaced with an algebraic relationship. The governing equations then correspond to mass conservation and momentum conservation in two components. Higher order elements (the C^0 cubic on triangles) were employed with two algorithm classes:

- (a) Implicit time marching code for the unsteady equations (ref. 17), and

(b) Block iterative solution of nonlinear systems of algebraic equations arising from FEM models of the steady governing equations (ref. 5).

Linear triangular element quasi-explicit time marching schemes were applied to the full Navier-Stokes equations for the following cases:

(c) (Perhaps) academic calculation in rectangular coordinates of an oblique shock in otherwise uniform flow, using inconsistent (lumped) linear element schemes, and

(d) Calculations in axis-symmetric cylindrical coordinates of the boattail afterbody problem with embedded weak shocks and recirculation.

The purpose of this paper is to discuss some of the assets and liabilities of FEM in fluid dynamic application; to summarize some of the findings of this investigation; and to report more fully upon the phase of the investigation concerning linear elements and the complete Navier-Stokes equations, codes (c) and (d).

The Advantages of FEM

Before consideration of the adverse features of FEM, we consider briefly some of its so-called advantages; these are generally considered in the literature to be:

- (a) Variable gridworks, allowing economy of grid point allocation;
- (b) Possible triangular elements, allowing complex (non-linear) boundaries to be fit readily;
- (c) Higher order elements, allowing greater accuracy;
- (d) Typically easier handling of boundary conditions; and
- (e) Accurate and reliable results from algorithms which leave little choice of the way in which individual equation terms are differenced.

The survey paper of Roache (ref. 1) provides a fairly unbiased examination of these characteristics of FEM methods, some points of which may be repeated here, together with some additional observations based on results included in the present paper.

Variable grid capability and fitting of curved boundaries together with accurate final results appear to be the greatest assets of FEM. There may be classes of particular problems where the cost of these assets is reasonable; but such probably do not include the class with geometry amenable to reform by means of stretching transformations in one or more variables. Even so, to make use of this asset, in addition to the costs already discussed some device for automatic choice of the grid point placement is necessary in order to eliminate enormous manual labor and human error. The stretching transformation utilized by Holst (ref. 18) which maps a uniform grid in the computational plane into an irregular grid in the physical plane can be considered ideal for such: The nonuniform grid so devised is, of course, topologically equivalent to a rectangular grid for which a mesh generator is particularly simple to code. Thus, the grid point selection device is readily automated and parameters easily adjustable to position the grid points where they are required for resolution. If such a device is needed to assure proper placement of nodes, we are a small step from transforming the equations and obviating the advantages (a) and (b).

The advantage of higher order elements is not as real as is often claimed in FEM literature, since the additional computation induced offsets the reduction in grid points. Moreover, this reduction is not as monumental as one might perceive (going from linear to cubic elements might cut a 1000-point grid to one having 600-700 nodal variables without much difference in accuracy). However, from personal experience the cubic element code can be around a factor of six or eight times slower than the linear element code.

Finally, boundary conditions are usually no easier to treat unless higher order elements which carry derivatives as nodal point variables are used. If such is the case, derivative boundary conditions are no different from function boundary conditions, in some cases. Depending upon the finite element algorithm involved, some computational boundary conditions which are fairly easy to implement in FDM may now cause difficulties in the FEM implementation. For example, if we are implicit time marching with symmetric positive definite matrices to invert, the application of computational boundary conditions such as linear or quadratic extrapolation destroys the matrix symmetry and thus leads to more troublesome equation solving.

The Adverseness of Finite Elements in Fluid Dynamics

Perhaps it may be useful to enumerate some difficulties which are to be expected in computational fluid dynamics. For problems governed by the Navier-Stokes equations, several coupled second order partial differential equations in two or more space dimensions are to be solved. The calculation of mixing or separated flows with recirculation and possible embedded shocks and boundary layer regimes in regions with curved boundaries require for economy irregular grids. As is usually the case, the several sets of dependent flow variables coupled with mesh refinement sufficient for problem resolution demands from several hundred to several thousand nodal point variables. (For example, a coarse mesh for the boattail afterbody problem discussed herein requires 1681 grid points (41×41 mesh) and 6724 nodal variables (4 equations) to be time marched to steady state.) Furthermore, for problems with chemical reactions involved, the number of governing equations increases still more, and the equation set of the numerical model is usually stiff.

For such huge calculations, applications experience seems to promote a tendency to the axiom of simplicity: the more complicated the problem from the viewpoint of number of equations, number of grid points necessary, etc., the less likely is an economically successful solution by means of the more refined numerical model (the implicit schemes with high order of accuracy), due simply to the sheer mass of calculations involved, computer storage requirements, and complexity of the coding.

Indeed, the advent of the vector computer has indicated that for certain problem size ranges the simple explicit time marching schemes with restrictive stability limitations surpass the theoretically unconditionally stable implicit schemes in overall machine economy. Consequently, for time asymptotic marching implicit schemes have of late fallen more out of favor, although this is not the case for one-space coordinate marching as for the parabolized Navier-Stokes flows (ref. 19).

It appears from the present study that in general time marching even the simpler finite element schemes are more cumbersome to implement and in turn less economical than is the average finite difference scheme of comparable accuracy. This is due largely to the global nature of the function approximation as well

as to the more general scope of the FEM method in terms of gridwise applicability (even with regular grids the method of programming generally does not deviate a great deal from that for the irregular grid), as well as the averaging process the FEM employs in discretizing space derivative terms (ref. 20). Further time-consuming function evaluations result from the need to evaluate finite element area integrals by means of quadrature schemes (ref. 15) when nonlinear terms are present. Some of the adverseness of the finite element method will now be further elucidated.

Relationship Between FEM and FDM Discretizations

The Linear Element Model. Consider the problem of modeling the vorticity transport equation (u and v assumed constant)

$$\frac{\partial q}{\partial t} + u \frac{\partial q}{\partial x} + v \frac{\partial q}{\partial y} = \nu \left(\frac{\partial^2 q}{\partial x^2} + \frac{\partial^2 q}{\partial y^2} \right) \quad (1)$$

employing a linear element finite element model.

Let $\{\phi_J(x,y): J = 1, 2, \dots, N\}$ be the triangular element piecewise linear shape functions associated with the nodes of a triangulated domain (see figure 1). These shape functions are defined on a triangle with vertices at points (x_P, y_P) , (x_Q, y_Q) , (x_R, y_R) by the equations

$$\begin{aligned} \phi_P &= a_P + b_P x + c_P y \\ a_P &= 1 - (b_P x_P + c_P y_P) \\ b_P &= y_Q - y_R = y_{QR} \\ c_P &= x_R - x_Q = x_{QR} \end{aligned} \quad (2)$$

The finite element model equation at node point J as produced by the Galerkin technique is

$$\int_{\Omega} \phi_J \frac{\partial q}{\partial t} dA = - \int \int_{\Omega} \left\{ \phi_J \left[u \frac{\partial q}{\partial x} + v \frac{\partial q}{\partial y} \right] + v \left[\frac{\partial \phi_J}{\partial x} \frac{\partial q}{\partial x} + \frac{\partial \phi_J}{\partial y} \frac{\partial q}{\partial y} \right] \right\} dA$$

$$+ \oint_{\Gamma} \phi_J \left[\frac{\partial q}{\partial x} dy - \frac{\partial q}{\partial y} dx \right] \quad (3)$$

FEM Equations on a Nonuniform Grid. Expanding q in terms of nodal values q_J in the form

$$q = \sum_{J=1}^N q_J(t) \phi_J(x,y)$$

and substituting in equation (3) we obtain the interior point discretized finite element equation associated with node point J which will now be indicated (refer to figure 1). Here

$$\dot{(\quad)} = \frac{\partial}{\partial t} (\quad),$$

$\langle (\quad) \rangle$ = the corresponding finite element discretization of term (\quad) of equation (1), and

A_i = area of triangle i

The contributions to the equation at node J are

Time term

$$\begin{aligned} \langle \frac{\partial q}{\partial t} \rangle &= \dot{q}_J (A_1 + A_2 + A_3 + A_4 + A_5 + A_6) + \dot{q}_A \left(\frac{A_6 + A_1}{12} \right) \\ &+ \dot{q}_B \left(\frac{A_1 + A_2}{12} \right) + \dot{q}_C \left(\frac{A_2 + A_3}{12} \right) + \dot{q}_D \left(\frac{A_3 + A_4}{12} \right) \\ &+ \dot{q}_E \left(\frac{A_4 + A_5}{12} \right) + \dot{q}_F \left(\frac{A_5 + A_6}{12} \right) \end{aligned} \quad (4)$$

X-diffusion term

$$\begin{aligned}
 \left\langle \frac{\partial^2 q}{\partial x^2} \right\rangle = & \frac{q_J}{4} \left[\frac{y_{AB}^2}{A_1} + \frac{y_{BC}^2}{A_2} + \frac{y_{CD}^2}{A_3} + \frac{y_{DE}^2}{A_4} + \frac{y_{EF}^2}{A_5} + \frac{y_{FA}^2}{A_6} \right] \\
 & + \frac{q_A}{4} \left[\frac{y_{FA} y_{JF}}{A_6} + \frac{y_{AB} y_{BJ}}{A_1} \right] + \frac{q_B}{4} \left[\frac{y_{AB} y_{JA}}{A_1} + \frac{y_{BC} y_{CJ}}{A_2} \right] \\
 & + \frac{q_C}{4} \left[\frac{y_{BC} y_{JB}}{A_2} + \frac{y_{CD} y_{DJ}}{A_3} \right] + \frac{q_D}{4} \left[\frac{y_{CD} y_{JC}}{A_3} + \frac{y_{DE} y_{EJ}}{A_4} \right] \\
 & + \frac{q_E}{4} \left[\frac{y_{DE} y_{JD}}{A_4} + \frac{y_{EF} y_{FJ}}{A_5} \right] + \frac{q_F}{4} \left[\frac{y_{EF} y_{JE}}{A_5} + \frac{y_{FA} y_{AJ}}{A_6} \right]
 \end{aligned} \tag{5}$$

Y-diffusion term

In equation (5) replace x by y and maintain subscripts, q values as written. Here $y_{PQ} = y_P - y_Q$, etc. (6)

X-convection term

$$\begin{aligned}
 \left\langle u \frac{\partial q}{\partial x} \right\rangle = & \frac{u}{6} \{ q_J (y_{AB} + y_{BC} + y_{CD} + y_{DE} + y_{EF} + y_{FA}) \\
 & + q_A (y_{JF} + y_{BJ}) + q_B (y_{JA} + y_{CJ}) + q_C (y_{JB} + y_{DJ}) \\
 & + q_D (y_{JC} + y_{EJ}) + q_E (y_{JD} + y_{FJ}) + q_F (y_{JE} + y_{AJ}) \}
 \end{aligned} \tag{7}$$

Y-convection term

Rewrite equation (7) with x and y interchanged, but retaining all q_J and all subscripts as at present. (8)

FEM Equations on Uniform Grid. It is of interest to observe that for a uniform grid with

$$x_P - x_Q = \pm \Delta x, \quad y_P - y_Q = \pm \Delta y,$$

the suitable addition of terms (1-8) produces the discretized finite element (central space differenced) equations

$$\begin{aligned}
\frac{1}{12} \left\{ 6\overset{\circ}{q}_{I,J} + \overset{\circ}{q}_{I-1,J} + \overset{\circ}{q}_{I+1,J} + \overset{\circ}{q}_{I,J-1} + \overset{\circ}{q}_{I,J+1} + \overset{\circ}{q}_{I+1,J+1} \right. \\
\left. + \overset{\circ}{q}_{I-1,J-1} \right\} = -\frac{u}{6} \left\{ \left(\frac{q_{I,J-1} - q_{I-1,J-1}}{\Delta x} \right) \right. \\
\left. + 2 \left(\frac{q_{I+1,J} - q_{I-1,J}}{\Delta x} \right) + \left(\frac{q_{I+1,J+1} - q_{I,J+1}}{\Delta x} \right) \right\} \\
- \frac{v}{6} \left\{ \left(\frac{q_{I-1,J} - q_{I-1,J-1}}{\Delta y} \right) + 2 \left(\frac{q_{I,J+1} - q_{I,J-1}}{\Delta y} \right) \right. \\
\left. + \left(\frac{q_{I+1,J+1} - q_{I+1,J}}{\Delta y} \right) \right\} + v \left\{ \left(\frac{q_{I+1,J} - 2q_{I,J} + q_{I-1,J}}{(\Delta x)^2} \right) \right. \\
\left. + \left(\frac{q_{I,J+1} - 2q_{I,J} + q_{I,J-1}}{(\Delta y)^2} \right) \right\}
\end{aligned} \tag{9}$$

Here we see that second space derivatives have been central differenced and first derivatives approximated with weighted averages of offset centered difference approximations. The inversion of the time derivative coefficient matrix before making the analysis would allow the observation that the space discretizations are all weighted averages of centered differenced terms.

Inconsistent FEM

Consider Roache's question (ref. 1)--what is a finite element method? From equations (4 to 8) we can see in this instance that a Galerkin method employing linear elements produces a space discretized finite difference scheme which is second order accurate and which possesses arbitrary variability in grid point location. Of course, for good results the triangles should not be too distorted, with in particular large obtuse angles not allowed, although small angle restrictions are not as significant as originally supposed (ref. 21). For uniform grids the method analyzed applies centered space differences to diffusion terms and weighted averages of such differences to convection terms.

When applied to transient problems the method is inherently implicit. It produces systems of ordinary differential equations coupling nodal variable time derivatives which are of the form

$$B \frac{d\bar{Q}}{dt} = f(\bar{Q}) \quad (10)$$

Should one wish to numerically integrate employing explicit schemes, equation (10) presents a matrix inversion barrier at the outset, since B is banded and of significant bandwidth.

This implicitness can be avoided (observe in equation (4) the result of Taylor's expansions about the central point A) by lumping B to obtain an easily inverted diagonal matrix, according to the relations

$$D_{ii} = \sum_j B_{ij} ; \quad D_{ij} = 0 , \quad i \neq j . \quad (11)$$

On a uniform grid the lumped system

$$\frac{d\bar{Q}}{dt} = D^{-1} \bar{f}(\bar{Q}) \quad (12)$$

is consistent except near the boundaries. For a nonuniform grid the lumping process globally lowers to first order the accuracy of the transient solution. However, for uniform grids this occurs only near the boundaries.

This deterioration in accuracy on nonuniform grids is a compelling argument against lumping. For this reason the technique of simplifying geometry by stretching transformations with uniform mesh FEM applied in the transformed plane gains some favor. However, why do the discretization with an FEM, considering its chief advantage is complex geometry capacity and that furthermore it always applies centered differencing to convection terms? Historically, the *raison d'être* for the evolution of the Lax-Wendroff type method is to obtain second order accuracy while at the same time preserving the stability characteristics of the upwind techniques. As traced by

Roache (ref. 22) this historical evolution involved successive improvements over the forward time central space method via DuFort Frankel, the upwind methods, Lax-Wendroff methods, in that order. The cumbersomeness of applying upwind differencing with FEM seems to exclude such a similar chain of evolution; this type of differencing does not appear to be naturally inherent in FEM discretizations (ref. 20).

Extra Stiffness of FEM Systems

Consider equation (9) with convection terms omitted. A Von Neuman-Fourier resolution

$$q(x,y,t) = C(t) \exp[i(\xi x + \eta y)] , \quad i = \sqrt{-1} \quad (13)$$

then produces the amplitude evolution characterized by

$$\frac{dC}{dt} = \alpha \lambda C . \quad (14)$$

Here ξ , η are frequency related, α results from time derivative coupling,

$$\lambda = -4 \left[\frac{\sin^2 \left(\frac{\xi \Delta x}{2} \right)}{(\Delta x)^2} + \frac{\sin^2 \left(\frac{\eta \Delta y}{2} \right)}{(\Delta y)^2} \right] v \quad (15)$$

and

$$\alpha = \frac{2}{\left[1 + \frac{1}{3} (\cos \xi \Delta x + \cos \eta \Delta y + \cos (\xi \Delta x + \eta \Delta y)) \right]} \quad (16)$$

Letting

$$\lambda' = \alpha \lambda , \quad \lambda = \xi = \eta , \quad \Delta x = \Delta y , \quad \theta = \lambda \Delta x ,$$

we may deduce that

$$\frac{\text{Max}}{\theta} |\lambda'| \approx \frac{28\nu}{(\Delta x)^2} \quad (17)$$

while

$$\frac{\text{Max}}{\theta} |\lambda| = \frac{8\nu}{(\Delta x)^2} \quad (18)$$

Hence the time derivative coupling has produced a stiffer system by a factor of approximately 3.5 than would an ordinary FDM method with centered space differencing. Considering the assumptions of the analysis, this is in excellent agreement with the experimental observations of a factor of three or four (ref. 23).

In terms of stability implications the forward time centered space FDM method applied to the diffusion equation is restricted by $(\Delta x = \Delta y)$

$$\beta = \nu \frac{\Delta t}{(\Delta x)^2} \leq \frac{1}{4} \quad (19)$$

whereas forward time differencing of equation (9) restricts the resulting FEM algorithm according to

$$\beta \leq \frac{1}{14} \quad (20)$$

Of course, the same considerations apply to equation (1), with extra complication.

Storage Considerations

It is clear the implicitness of FEM methods, if tolerated by avoiding any sort of lumping, will require extra storage. What is perhaps not so obvious is the storage cost resulting from the capability of totally irregular grid point location. The shape of triangular elements can be used to advantage in accurate fitting of curved boundaries; hence, transformations are not

essential in this respect. However, some penalties for this generality are necessary; most notably, the increased grid disorder requires increased storage of information concerning grid character, such as node coordinates and their triangle associations.

For example, on a 41×41 grid with 3200 triangular elements the storing of 4 bits of information per triangle (node numbers of three vertices and boundary triangle indicator) requires 12800 storage locations. (In contrast, on an FDM mesh the reference point at which a difference equation is to be written is located by the I, J indices inside a nested DO loop, with index incrementation for determining neighbor points; consequently, no storage of grid information of the above type is necessary.) Moreover, indication of whether each node is unrestricted (is there an equation to be written or not?) requires 6724 bits of information, on the 41×41 grid with 4 dependent variables per node.

For the implicit case

$$B \frac{d\bar{Q}}{dt} = \bar{f}(\bar{Q}) , \quad (21)$$

with linear triangular elements and the 41×41 grid B is a symmetric banded matrix of bandwidth 83, of dimension 1681×1681 . Moreover, one such system is required for each of the four fluid dynamic dependent variables. Problems of this size necessitate out-of-core solving with associated buffer needs. For this grid the split-band Cholesky method (ref. 24) (see Appendix I) requires a buffer of minimum size 9000 words for inversion of B , with $4 \times 1681 = 6724$ storage locations for \bar{f} . Out-of-core frontal methods require less storage (refs. 25, 26), but would seem more time consuming on a per step basis since their implementation would necessarily require inversion of the matrices involved every time step. Frontal utilization would appear to have as a corequisite a fully implicit time integration procedure. This appears vastly more complex to implement than the split-band Cholesky method in which B is inverted only once with subsequent front and back solves utilized whenever $\frac{d\bar{Q}}{dt}$ is needed.

The picture emerging is that finite element implicitness and variable grid generality tends to cumbersome application and more heavy core storage requirements than is characteristic of finite difference methods (with MacCormack's method on the lower end of the spectrum and ADI the higher end). As regards the cumbersomeness of FEM, the device of time step doubling (ref. 18) which cuts total computer time a factor of 2.5 to 4 with MacCormack's method would be difficult or impossible to apply with quasi-explicit nonlumped or fully implicit FEM, due to system nodal variable coupling.

Time Considerations

It is clear from equations (4 to 8) that equation assembly time for the variable grid difference scheme probably should exceed by an order of magnitude that of a uniform grid scheme, particularly for the FDM technique where one numerical coefficient may receive from two to six contributions from separate sources. Furthermore, the estimate represented by this academic example is clearly optimistic; for the primitive variable Navier-Stokes problems practically every equation term exhibits nonlinearity, often to the extent that the algebraic manipulation impedes or the type of nonlinearity prevents a priori tabulation of the simplest form of the expression evaluated. Such evaluation is accomplished by calculating area integrals over elements of the geometrical domain by quadrature schemes (which with higher order function approximation can involve several quadrature points per element, if one is not to degrade the order of accuracy otherwise expected (ref. 15)).

Note from equations (4 to 8) that each additive term in an equation coefficient represents a contribution from a separate triangular element. This is the key to the FEM equation assembly concept; one proceeds triangle by triangle computing contributions to all equations associated with nodes of each triangle, adding each contribution into the proper place. It is this equation assembly process which consumes the greatest relative computation time through function evaluation for the numerous contributions to one coefficient.

When the governing equations are largely composed of linear terms, as for stream function-vorticity formulations or some potential flow situations, with troublesome a priori algebraic manipulation the matrix

element contributions can be reduced to simplest possible form for rapid evaluation, as done by Bratanow (ref. 23) and Baker (ref. 4). Such a scheme represents some improvement over the machine quadrature approach; however, it is clearly impractical for higher order elements and/or highly nonlinear equations such as primitive variable Navier-Stokes. In any event this algebraic manipulation represents further cumbersomeness in application.

Here one is impressed that even though geometric stretching transformations may increase the number of terms in the governing equation set, depending upon the complexity of nonlinear coefficient evaluations the resulting FDM application on a uniform grid appears should have much leeway in central processor time (due to simpler equation assembly) over FEM applied on the original domain. Moreover, the FDM transformation approach exactly accounts for boundary curvature, while FEM boundary approximation by triangular elements actually introduces possible second order roughness effects.

FINITE ELEMENT MODEL OF NOZZLE AFTERBODY VISCOUS INTERACTION EFFECTS WITH PLUME SIMULATION

Flow separation has serious consequences in many fluid dynamics applications. Once separation occurs at the boundary of a submerged body, the resulting flowfield behavior departs radically from that predicted by the inviscid flow theory, because now the separating stream causes effectively the formulation of a new flow boundary. This added irregularity of the effective body geometry due to flow reversal and recirculation with resulting downstream turbulent wake can produce a relatively large increase in total vehicle drag.

Current interest in reducing aircraft drag is evidenced by the appearance in the literature of large amounts of experimental data and investigative study of various features of the problem. The difficulty of experimentally predicting the flow characteristics of a particular body geometry, due to the hot jet exhaust plume and Reynolds number scale effects, points to the need for accurate numerical simulation procedures. Calculations for the most general free plume case are not known to the author. However, for certain nozzle pressure ratios the plume simulator (see figure 2) produces results .

close to free plume results (ref. 18). The simulated flow field contains many of the same features as the free plume flowfield: separation and recirculation; separation shock; turbulent boundary layer on the boattail; and a turbulent recirculating region.

For the plume simulator MacCormack's FDM method has proven to be a notably successful numerical simulation device (ref. 18). It provides a computationally feasible tool which allows insight into the viscous/inviscid problem interactions, without the encumbrances characteristic of the weak interaction techniques which iteratively calculate separate solutions in the boundary layer and inviscid flow regimes, with consequent matching difficulties at common boundaries. The flow and geometry characteristics of the problem as well as availability of FDM results make it a good test case for comparative performance of FEM/FDM technology.

The subsequent sections of the present paper are addressed to the development of FEM algorithms for the solution of viscous compressible flow problems with possible embedded shocks and recirculation regions. As a logical first step in the development of such a computer code we consider the calculation in Cartesian coordinates of uniform flow on a rectangular region which encounters an embedded oblique shock with known turning angle. Having control at the boundary of the location at which the shock is introduced allows fairly accurate knowledge of where the shock should form (see figure 3). The code so developed then allows reasonably simple modification for computation of the boattail plume simulator problem, couched in axis-symmetric cylindrical coordinates. In both cases laminar flow is assumed; however, simple eddy viscosity or two layer turbulence models could be easily introduced.

The Navier-Stokes Equations

The equations governing the flow of a compressible viscous fluid in the absence of body forces and electromagnetic effects can be written in weak conservation law form as follows:

$$\frac{\partial U}{\partial t} + \frac{\partial F}{\partial x} + \frac{\partial G}{\partial y} + H = 0 \quad (22)$$

Nondimensionalizing the governing equations using free stream density (ρ_∞), free stream x-direction velocity (u_∞), boattail exit diameter (D_e), and reference temperature

$$T_{\text{Ref}} = \frac{u_\infty^2}{C_v} \quad (23)$$

the following dimensionless equations hold:

Cartesian Coordinates

$$U = \begin{bmatrix} \rho \\ \rho u \\ \rho v \\ E \end{bmatrix} \quad (24)$$

$$F = \begin{bmatrix} \rho u \\ \rho u^2 + P - \tau_{xx} \\ \rho uv - \tau_{xy} \\ (E + P - \tau_{xx})u - \tau_{xy}u + Q_x \end{bmatrix} \quad (25)$$

$$G = \begin{bmatrix} \rho v \\ \rho uv - \tau_{xy} \\ \rho v^2 + P - \tau_{yy} \\ (E + P - \tau_{yy})v - \tau_{xy}v + Q_y \end{bmatrix} \quad (26)$$

$$H = \begin{bmatrix} 0 \\ 0 \\ 0 \\ 0 \end{bmatrix} \quad (27)$$

Here the viscous stress relations are

$$\left. \begin{aligned} \tau_{xx} &= \frac{\mu}{R_e} \left(\frac{4}{3} \frac{\partial u}{\partial x} - \frac{2}{3} \frac{\partial v}{\partial y} \right) \\ \tau_{xy} &= \frac{\mu}{R_e} \left(\frac{\partial u}{\partial y} + \frac{\partial v}{\partial x} \right) \\ \tau_{yy} &= \frac{\mu}{R_e} \left(\frac{4}{3} \frac{\partial v}{\partial y} - \frac{2}{3} \frac{\partial u}{\partial x} \right) \end{aligned} \right\} \quad (28)$$

and the heat flux components are

$$\left. \begin{aligned} Q_x &= - \frac{k\gamma}{P R_e} \frac{\partial T}{\partial x} \\ Q_y &= - \frac{k\gamma}{P R_e} \frac{\partial T}{\partial y} \end{aligned} \right\} \quad (29)$$

The nondimensionalized constitutive relationships are Sutherlands viscosity law

$$\mu = T^{3/2} \left(\frac{1+S}{T+S} \right) ; \quad (30)$$

the perfect gas law

$$P = (\gamma - 1)\rho T ; \quad (31)$$

and the specific total energy definition,

$$E = \rho \left(T + \frac{u^2 + v^2}{2} \right) . \quad (32)$$

Also

$$s = \frac{198.6}{T_{\text{Ref}}}$$

k = thermal conductivity

R_e = Reynolds number

P_R = Prandtl's number

ρ = density

u = x-component of velocity

v = y-component of velocity

P = static pressure

T = temperature

$\gamma = 1.4$

μ = viscosity

Axis-symmetric Cylindrical Coordinates

Using the previously described nondimensionalization, with x the axial and y the radial direction, the equations completing definition of the governing equations in axis-symmetric coordinates are given below. The constitutive relationships are as previously defined, as well as the heat flux expressions. However, the following equation changes are necessary:

$$\bar{H} = \begin{bmatrix} 0 \\ 0 \\ -P + \tau_{\theta\theta} \\ 0 \end{bmatrix} \quad \left. \begin{array}{l} \bar{U} = yU \\ \bar{G} = yG \\ \bar{F} = yF \end{array} \right\} \quad (33)$$

Viscous stresses

$$\left. \begin{array}{l} \bar{\tau}_{xx} = \frac{4\mu}{3R_e} \frac{\partial u}{\partial x} - \frac{2}{3} \frac{\mu}{R_e} \left(\frac{\partial v}{\partial y} + \frac{v}{y} \right) \\ \bar{\tau}_{yy} = \frac{2\mu}{3R_e} \left[2 \frac{\partial v}{\partial y} - \left(\frac{\partial u}{\partial x} + \frac{u}{y} \right) \right] \\ \bar{\tau}_{xy} = \frac{\mu}{R_e} \left[\frac{\partial u}{\partial y} + \frac{\partial v}{\partial x} \right] \\ \bar{\tau}_{\theta\theta} = \frac{2\mu}{3R_e} \left[2 \frac{v}{y} - \left(\frac{\partial u}{\partial x} + \frac{\partial v}{\partial y} \right) \right] \end{array} \right\} \quad (34)$$

The Galerkin FEM Equations

The first step in the FEM discretization of equation (22) is the triangulation of the computational domain D with boundary Γ . Spatially piecewise linear function approximation is accomplished by associating shape functions of the form indicated by equation (2) with each vertex of a triangle. Trial functions are given by

$$U(x,y,t) = \sum_{J=1}^N U_J(t) \phi_J(x,y) \quad , \quad (35)$$

where U_J is the four component vector specifying the value of the vector (23) at the J -th node, and N is the total number of nodes.

The value of $U_J(t)$ is determined using the Galerkin technique by forcing for every node at which a component of U_J is not specified

by a boundary condition the corresponding component of the (Galerkin) equation

$$\begin{aligned} \iint_{\Omega} \phi_J \frac{\partial U}{\partial t} dA = \iint_D \left[F \frac{\partial \phi_J}{\partial x} + G \frac{\partial \phi_J}{\partial y} - \phi_J H \right] dx dy \\ + \int_{\Gamma} \phi_J [G dx - F dy] \end{aligned} \quad (36)$$

to hold. This yields four coupled systems of ordinary differential equations

$$[A_i] \frac{\partial \bar{q}_i}{\partial t} = f(\bar{q}_i) , \quad i = 1, 2, 3, 4 \quad (37)$$

to be time integrated. Here

$$[A_i]_{JK} = \iint_D \phi_J \phi_K dA \quad (38)$$

and \bar{q}_i is the collection of all nodal values of component i of the vector (23) which are allowed to vary with time.

The time integration of equation (30) is accomplished using the explicit self-starting maximally stable predictor-corrector algorithms of reference 27. For the oblique shock calculations the matrices A_i of equation (30) were lumped by the procedure of equation (11) to avoid the inversion. Integrals over a triangle arising from the left member of equation (36) are a priori exactly evaluated as

$$\iint_{Ti} \phi_J \phi_K dA = \begin{cases} \frac{A}{6} , & J = K \\ \frac{A}{12} , & J \neq K \end{cases} \quad (39)$$

where A is the area of triangle T_i . The integrals over triangles of the right member nonlinearities are evaluated by one point quadratures, with two point quadratures applied to the boundary integral terms. For the boattail afterbody calculations on a highly uniform grid (see figure 4) the inversion of the matrices in equation (30) is accomplished by developing a special purpose out-of-core equation-solving routine, the split band-Cholesky solver (see Appendix I).

A fourth order damping scheme is used to smooth oscillations resulting from shocks or other large flowfield gradients. The additive damping corrections employed are described in reference 18.

Boundary Conditions

The computational domain for the oblique shock calculation is shown in figure 3. Uniform flow conditions are prescribed on the inflow and prior to the point of introduction of the shock between nodes six and seven on the top boundary, including point seven and along the remainder of the top boundary altered uniform flow conditions corresponding to the flow having been turned by a shock at an incidence angle of 23 degrees are prescribed. Computational boundary conditions are applied along the bottom and outflow boundary; zero normal gradient ($f_2 = f_1$) along the bottom and linear extrapolation ($f_3 = 2f_2 - f_1$) on the outflow.

The computational domain for the boattail afterbody problem is shown in figure 4. The points of the rectangular appearing grid were obtained as in reference 18, where separate stretching in the two coordinate directions was employed in mapping the points in the physical plane (also the computational plane for the FEM calculation) onto the nodes of a uniform grid in the (transformed) computational plane. The parameters of the stretching mappings were chosen to concentrate more points along the wall and in the region of recirculation. The physical plane gridwork so obtained was triangulated for FEM purposes by drawing in the left-to-right and bottom-to-top diagonal of each rectangle. Thus, the mapping yields a readily automated grid generation technique.

The boundary conditions along the upper and outflow boundaries utilize linear extrapolation of interior point data for the variables ρ , u , v , T with E determined from equation (32). Along the wall pressure is linearly extrapolated; the no-slip condition specifies u, v ; and $T = T_w$ is specified; ρ , E then depend upon \underline{P} , T as specified by equations (31 to 32). (The validity of the linear extrapolation requires placement of the top and outflow boundaries sufficiently far removed from the boattail curvature, with the upper boundary essentially in free stream.) The flow conditions on inflow employ profiles obtained from a combination method of characteristics/boundary layer solution as described in reference 18.

NUMERICAL RESULTS

Oblique Shock Flow

The main purpose of the oblique shock calculations is to demonstrate for a problem with known solution the correctness of the finite element code and its applicability to flows involving shocks. Calculations are performed with Mach number $M = 3$ in the uniform flow, Prandtl number $P_R = 0.72$ and Reynolds numbers of 81 and 81,000. Table 1 shows the test conditions used to simulate the introduction of the shock between two grid points on the upper boundary. For the low Reynolds number, weak shock ($R_e = 80.869$) convergence was achieved in around 150 steps on a uniform 21×31 grid with $\Delta x = .05$, $\Delta y = .0333$ and $\Delta t = .01$. The criterion for convergence of calculations herein discussed is

$$|U_{n+1} - U_n| \leq 10^{-4}$$

for all components of U . No artificial viscosity was added.

For the crisp high Reynolds number ($R_e = 80,869$) shock mesh refinement became necessary. Since the shock did not penetrate the bottom half of the previous flow domain, this lower half was truncated and a 31×41 grid ($\Delta x = .0333$, $\Delta y = .0125$) imposed on the top half. Applying artificial

Table 1. Conditions for Oblique Shock Simulation.

| <u>Uniform Flow Conditions</u> | <u>Post Shock Conditions</u> |
|--------------------------------|------------------------------|
| $M = 3.0$ | $M = 2.75799$ |
| $\rho = 1.0$ | $\rho = 1.29341$ |
| $u = 1.0$ | $u = 0.96537$ |
| $v = 0.0$ | $v = -0.08159$ |
| $T = 0.19841$ | $T = 0.22034$ |

viscosity of strength $C_x = .1$, $C_y = .1$ (see reference 18) to damp spurious oscillations arising from the crispness of the shock, convergence was achieved in 1000 steps with $\Delta t = .001$.

Results for the high Reynolds number case are presented in figures 5(a to d), through comparisons between FEM and MacCormack's FDM method (ref. 18). For the FDM calculation the original 21×31 grid was employed; hence, the exaggerated overshoot exhibited in some instances by the FDM results should not from the present data be considered a liability of the method, but is probably the result of mesh coarseness. Figure 5(e) shows pressure contours over the computational domain. Note that pressure values have been multiplied by 1000. The roughly one percent error fluctuations in pressure which appear in the uniform flow in front and back of the shock are attributed possibly to the effects of lumping boundary error propagating downstream, or else to the error criterion not being strong enough to assure convergence of the calculation at the time of termination.

The introduction of the high Reynolds number shock at the top boundary is accomplished by imposing uniform flow conditions on the inflow and at every top boundary grid point through point six, with post shock values at point seven and thereafter. Hence, due to the linear element model the shock behavior along this boundary did not exhibit actual jump discontinuity; but rather, linear ramp function transition over the interval $.1667 \leq x \leq .20$. Similarly, due to the coarser grid the corresponding transition for the FDM calculations occurred over the larger interval $.15 \leq x \leq .20$. Effectively, neither calculation pinpoints shock intersection with the boundary, but both model the proper jump conditions across the smeared transition region corresponding to a shock at 23 degrees angle of incidence.

By drawing a straight line at 23 degrees angle of incidence and intersecting the top boundary at $x = .1667$, the intersection of this line with the grid lines $x = x_1$ should yield a y-value in close proximity to the theoretical shock jump location. The level line on figures 5(a and b) in which pressure and density ratios across the shock are plotted indicates this location. Hence, the calculations appear in good agreement with theoretical shock jump locus to within the limits of the accuracy with which this location can be specified.

Boattail Afterbody Flow With Separation

In reference 18 numerical solutions have been obtained for axis-symmetric boattail bodies with solid sting plume simulators, for several geometric configurations mostly from the family of boattails with circular arc generators. The accuracy of MacCormack's method has been verified for this class of computations by comparisons with wind tunnel results. Thus, one can confidently prove the FEM calculations by comparison with the corresponding FDM results.

The configuration chosen for the present calculation is as follows: the streamwise length of the computational domain is $x_{\max} = .688$ m ; exit diameter is $D_e = .0914$ m ; boattail radius of curvature is .894 m; boattail length is .229 m; boattail angle is $\beta = 14.8$ degrees. The inflow boundary is placed one maximum diameter of .159 m upstream of the beginning of boattail curvature, to escape feedback upstream (through the boundary layer) of boattail expansion effects. Grid point 8 in the x-direction is the first and grid point 26 the last grid point associated with boattail curvature. Characteristic parameters for the flow calculation are free stream condition $M_\infty = 1.3$, total temperature $T_{t,\infty} = 340^\circ\text{K}$, $\gamma = 1.4$, Prandtl number $P_R = 0.72$, reference Reynolds number $R_e = 12365$, reference temperature $T_{\text{ref}} = 432,883$, wall temperature $T_w = 311.4^\circ\text{K}$, $s = .4$.

In order to reduce central processor time requirements in the calculation of a typical boattail flowfield the FEM calculation was initialized with output from the MacCormack code which had been allowed to run several hundred steps. Even so, on the coarse mesh (41×41) the FEM program required another 400 steps to converge, with time step .0002. (Further calculations beginning with a flowfield obtained by reproducing the inflow at all downstream locations are underway, and will be reported if completed in this investigation period.)

Figures 6(a to e) exhibit comparisons of density, velocity, pressure and temperature profiles at various downstream stations, for the two computational methods. All profile stations except the first occur within the region of recirculation which is clearly exhibited. The FEM results do not seem to resolve as much of the finer details of the flow as the FDM results, although the overall disagreement between the two is not significant. Perhaps it may

be of interest to note that in the expansion region where the FEM physical plane grid is most irregular the disagreement is not as significant as in that portion of the recirculation region extending onto the plume simulator. Hence, the transformation approach with regular mesh calculations in the transformed plane appears to be able to more uniformly account for significant geometric transition effects. However, these calculations do appear to establish that the FEM method can accomplish well the job required in the original geometry. Hence, the future of the method, if any, in transient calculations, may lie in those areas where the transformation approach encounters difficulty; e.g., where the simple stretching transformations are not sufficient. Here one could envision channel flows with significant channel curvature and irregularity in cross section which varies with flow direction.

Comparisons of Computational Efficiency

In this section are presented some efficiency comparisons for cases in which a particular physical problem has been solved numerically by both FEM and FDM algorithms. No claims are made that the respective computer codes were as highly optimized as possible, or that different paths of algorithm design might not have produced varied results. Nor is the data for comparison as extensive as might be desired due to the general expense of generating finite element results. However, one might expect this data to predict the general characteristics typical of FEM/FDM resource economy.

Table 2 exhibits comparisons of particular indicators of computational efficiency. The methods studied together with references documenting precise algorithm formulation are as follows: for free shear layer flows (at $Re = 1000$) consistent implicit FEM algorithms for marching solution of the time transient (ref. 17) and nonlinear nontimelike block iterative solution (ref. 5) of the steady Navier-Stokes equations are compared with an alternating direction implicit (ADI) FDM method which employs upwind differencing of convection terms (ref. 28). Likewise, the consistent linear element FEM algorithm herein discussed is compared with MacCormack's nonsplit method which employed time step doubling (TSTD) (ref. 18), applied to boattail after-body calculations.

In all cases exhibited it may be emphatically concluded the FEM structure is far greater demanding of core storage and time per computational step

Table 2. Comparison of FEM/FDM Performance Characteristics.

| Method | Equation Dynamics | Number of Governing Equations ¹ | Flow Class | Total Problem Unknowns | Storage Kg | Cpu Time ² | Apparent Maximum Step Size | Steps to Convergence |
|-------------------------------------|-------------------|--|-------------|---|---|-----------------------|----------------------------|----------------------|
| | | | | (Number of Nodes * Number of Equations) | | Sec/Step/ | | |
| | | | | Total Unknowns | Total Unknowns (CDC-6600 Computer Time Units) | | | |
| C° Cubic | Transient | 3 | Shear Layer | 1884 | | .0763 | .03 | 150 |
| ADI | Transient | 3 | Shear Layer | 3000 | | .00125 | .3 | 30 |
| C° Cubic | Steady | 3 | Shear Layer | 1884 | | .0545 | NA | 15 |
| Consistent Linear Elements | Transient | 4 | Boattail | 6724 | .033 | .00178 | .0006 | |
| Nonsplit MacCormack with TSTD | Transient | 4 | Boattail | 6724 | .011 | .00031 ³ | .0046 | 650 coarse steps |
| Lumped Linear Elements ¹ | Transient | 4 | Boattail | 10404 | .0134 | .00108 | NA | NA |

¹ Data extrapolated from consistent linear element case by subtracting equation solve time from total step time, and buffer storage from total storage, 51 x 51 grid.

² All boattail calculations were performed on the CYBER 175 computer; all others on the CDC-6600 computer. To obtain equivalent cpu times for comparison, CYBER units of time have been converted to CDC-6600 units by employing a multiplicative factor of 2.5.

³ Total cpu time to convergence divided by total number of coarse steps required.

than is the FDM algorithm and appears to require a smaller step size. Of course, the most conclusive efficiency comparison that one can initiate is the measurement of total problem solution time, as dictated by maximum step size and number of steps to convergence. In this respect MacCormack's method with TSTD required only 650 coarse steps and 544.5 seconds of Cyber 175 computer time for convergence on the ($R_e = 12365$) boattail afterbody problem with a 41×41 grid. Here one coarse step is equivalent to several fine steps (ref. 18). Present indications are that the consistent linear element FEM code can run at a step size in the range .0004 to .0006. Knowing that TSTD cannot be used to speed the computation one can at best project an efficiency defect in total computation time of above an order of magnitude.

The best showing for the FEM method occurred for the free shear layer code formulated at the outset to solve the steady governing equations. Here the excessive time requirements on a per iterative step basis are offset by only a few steps being needed for convergence. However, even this performance was still not competitive with the ADI performance (ref. 28).

The per step cpu time requirement for the consistent linear element code was extrapolated to that needed for a lumped code by subtracting matrix inversion time; notably, forty percent of the total time needed per step. Hence, it appears that a lumped algorithm applied on a stretched domain could be as efficient as the consistent code on the original domain (or better).

CONCLUSIONS

The results of comprehensive numerical investigation concerning the basic capabilities of the finite element method as a tool for numerical calculations related to compressible flow problems indicate that it provides an accurate and reliable solution technique. However, the inherent ease with which variable grids and complex geometries can be handled is offset in most cases by a cumbersomeness in application which (in comparison to the better FDM methods) hinders economic calculations to the extent of rendering the method unfeasible, particularly for time marching solution of the more complex aerodynamic flow problems.

Fully explicit FEM algorithms on nonuniform grids are hindered by order of accuracy estimates, while due to spectrum broadening stemming from time derivative coupling quasi-explicit schemes are hampered by more rigid stability restrictions as well as matrix inversion at the outset. Such difficulties can be greatly alleviated by yielding to inherent FEM implicitness through use of implicit numerical integration, at the cost of matrix assembly and inversion each time step. Due to core storage requirements, for larger problems this approach is not at all feasible unless frontal equation assembly and solving is employed. It is hard to believe that such an approach would be competitive with the better finite difference methods, in particular since it has been observed in shear layer calculations that implicit methods can be in practice time step restricted to near the explicit CFL limit. However, frontal solution appears the most economical route to follow if the FEM method is employed as a time marching scheme. Of course, one might expect further increases in efficiency by time splitting the equations and applying one-dimensional finite elements to obtain FEM-ADI algorithms. However, the next question to consider is whether by such an approach the variable grid-complex geometry capability might not be weakened. It thus appears the greatest future of the method lies in problem areas where solutions of the steady governing equations are sought at the outset. Here the more rapid convergence expected of nonlinear nontimelike mathematical iteration processes appears to offset the high per step overhead of the method tending to more nearly provide economic competitiveness with FDM results.

The following major points have been established by this investigation: the strongest assets of the finite element method are its (a) capabilities for reliable and accurate calculation employing variable grids which readily approximate complex geometry and (b) capably adapt to the presence of diverse regions of large solution gradients. Complex flows with embedded shocks and regions of recirculation can be accurately calculated without the necessity of domain transformation. However, for sufficiently complex equations FEM time marching schemes as presently conceived do not appear able to compete economically with the better FDM algorithms of comparable accuracy, due largely to the sheer number of computations involved. Greater overhead

may be expected in terms of both computer resources and man-year efforts required to produce auxiliary routines such as grid generators and out-of-core solvers. Some inflexibility is associated with the method; e.g., upwind differencing is not naturally achievable with the general element, and time step doubling would be difficult or impossible to perform. Finally, the greatest weakness of the finite element approach is the total computer processing time and storage required for problem solution.

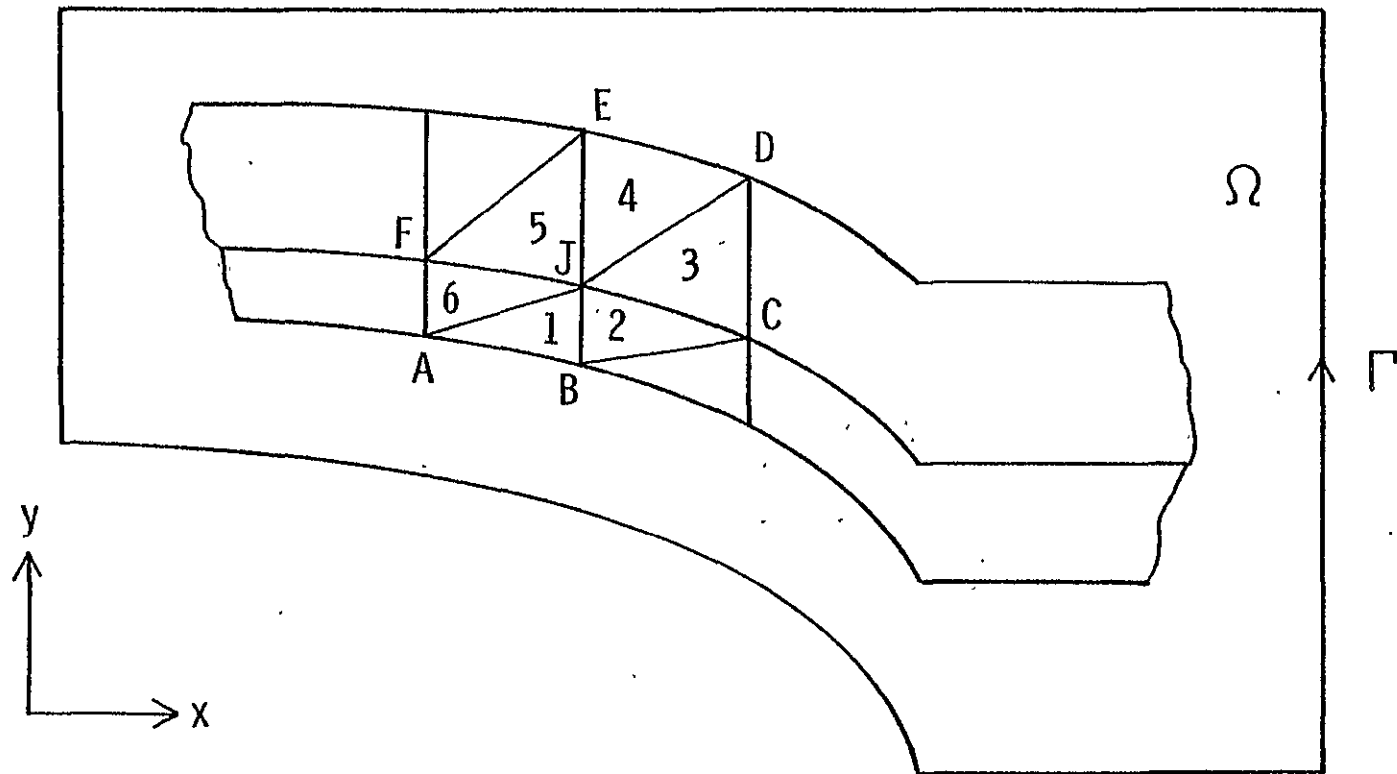


Figure 1. Finite element irregular triangulated gridwork.

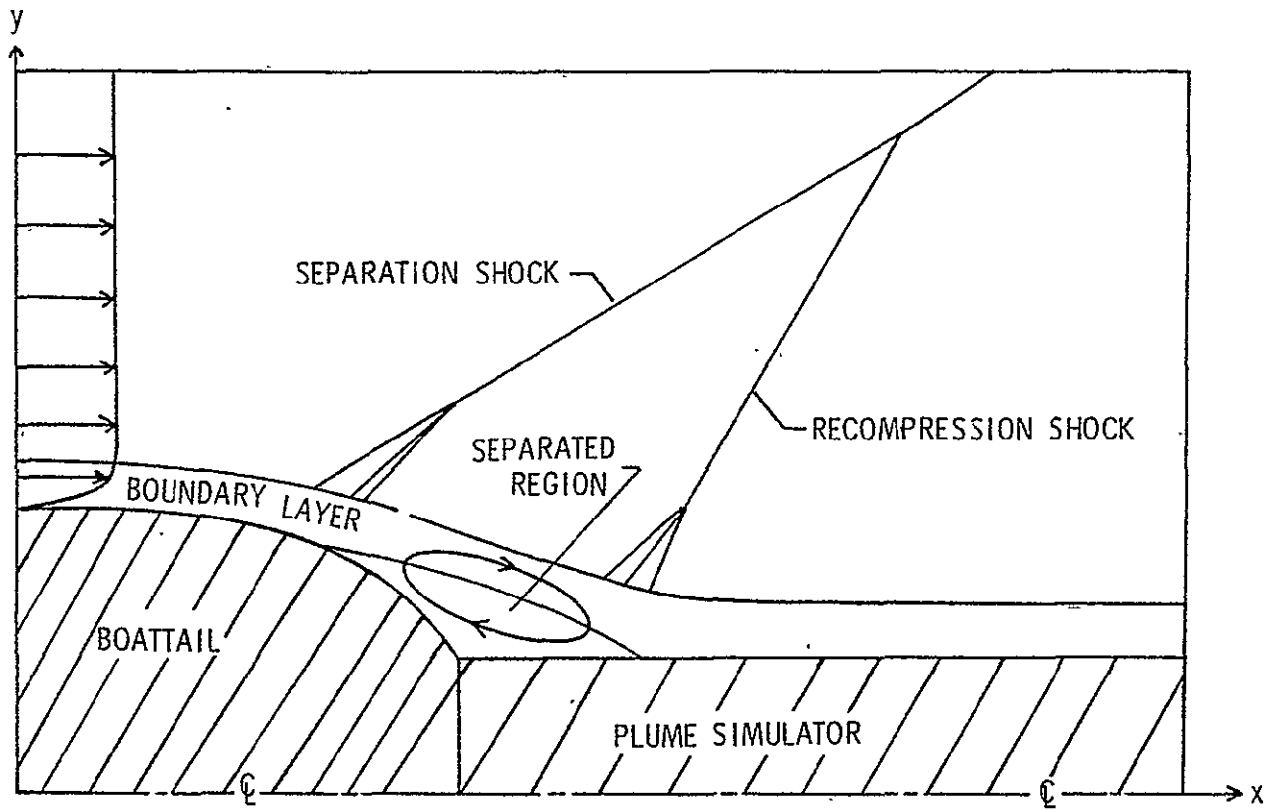


Figure 2. Boattail plume simulator flow field.

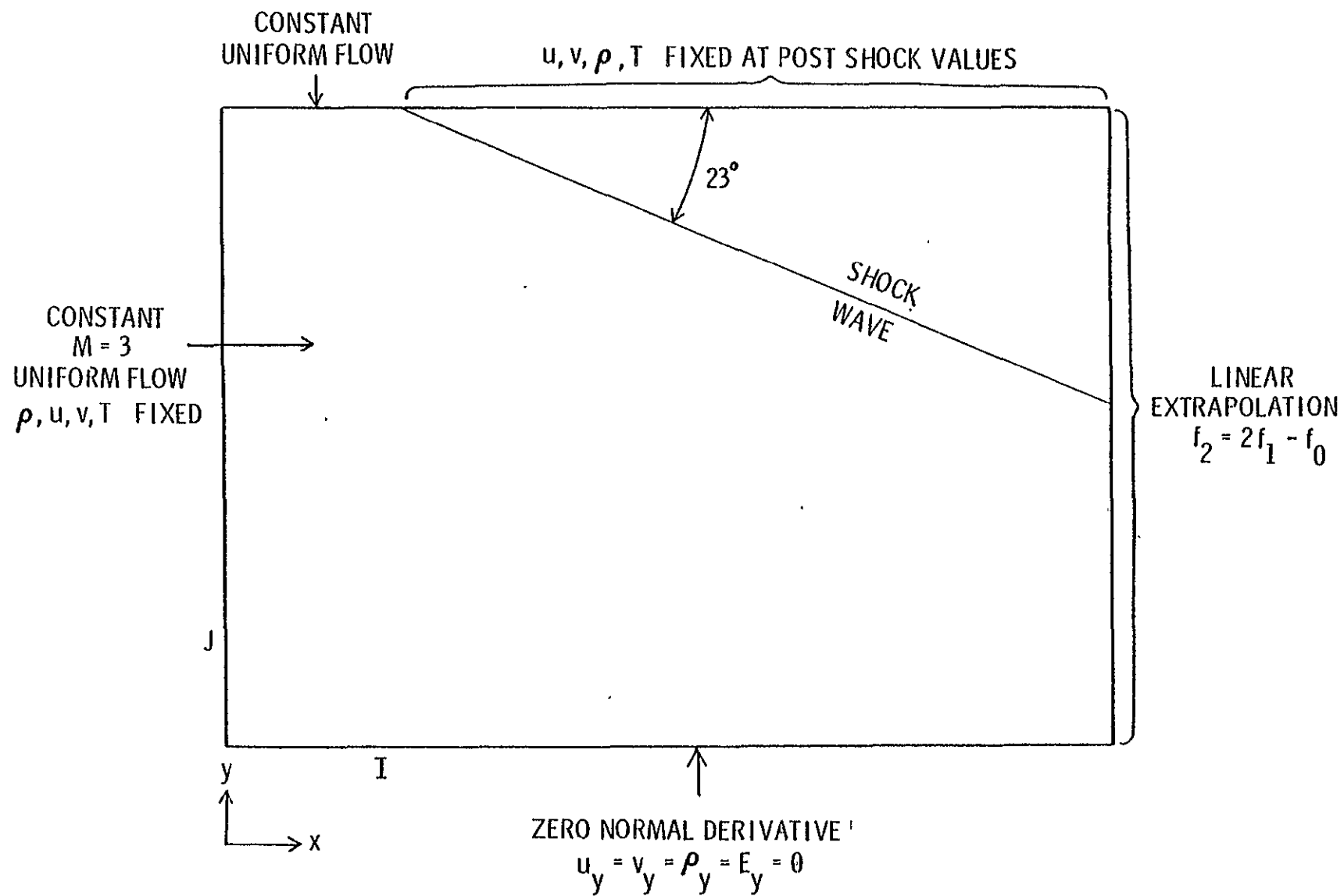


Figure 3. Oblique shock computational domain.

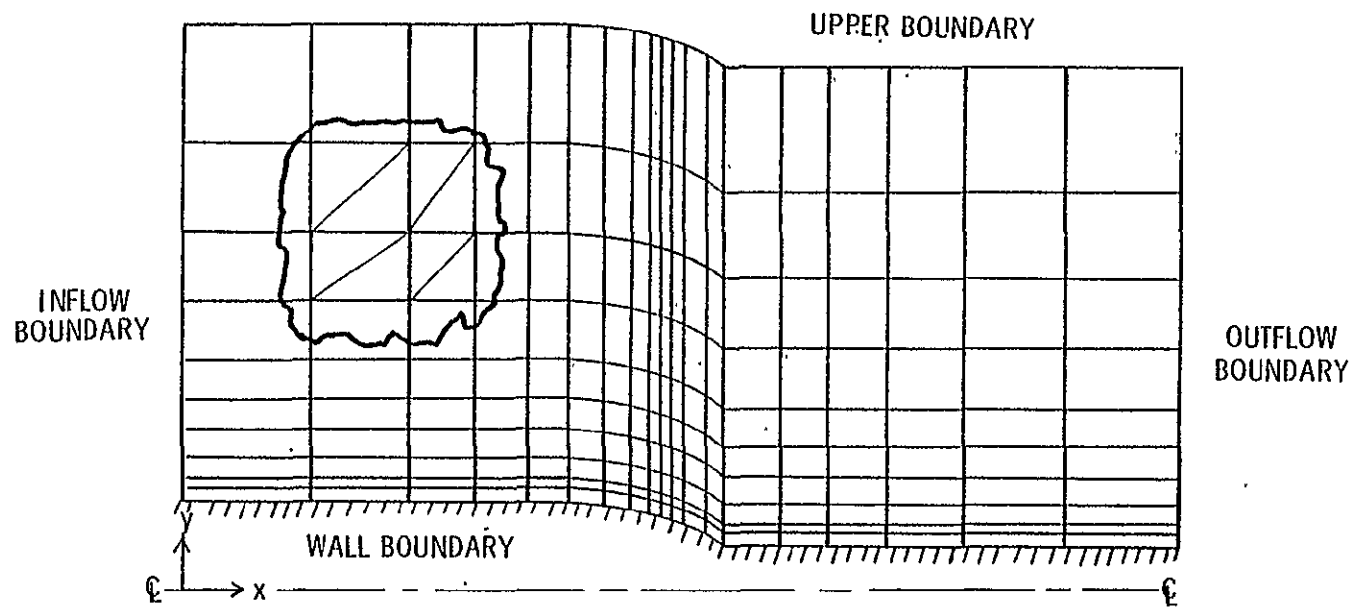


Figure 4. Boattail computational domain, with irregular triangular element formation.

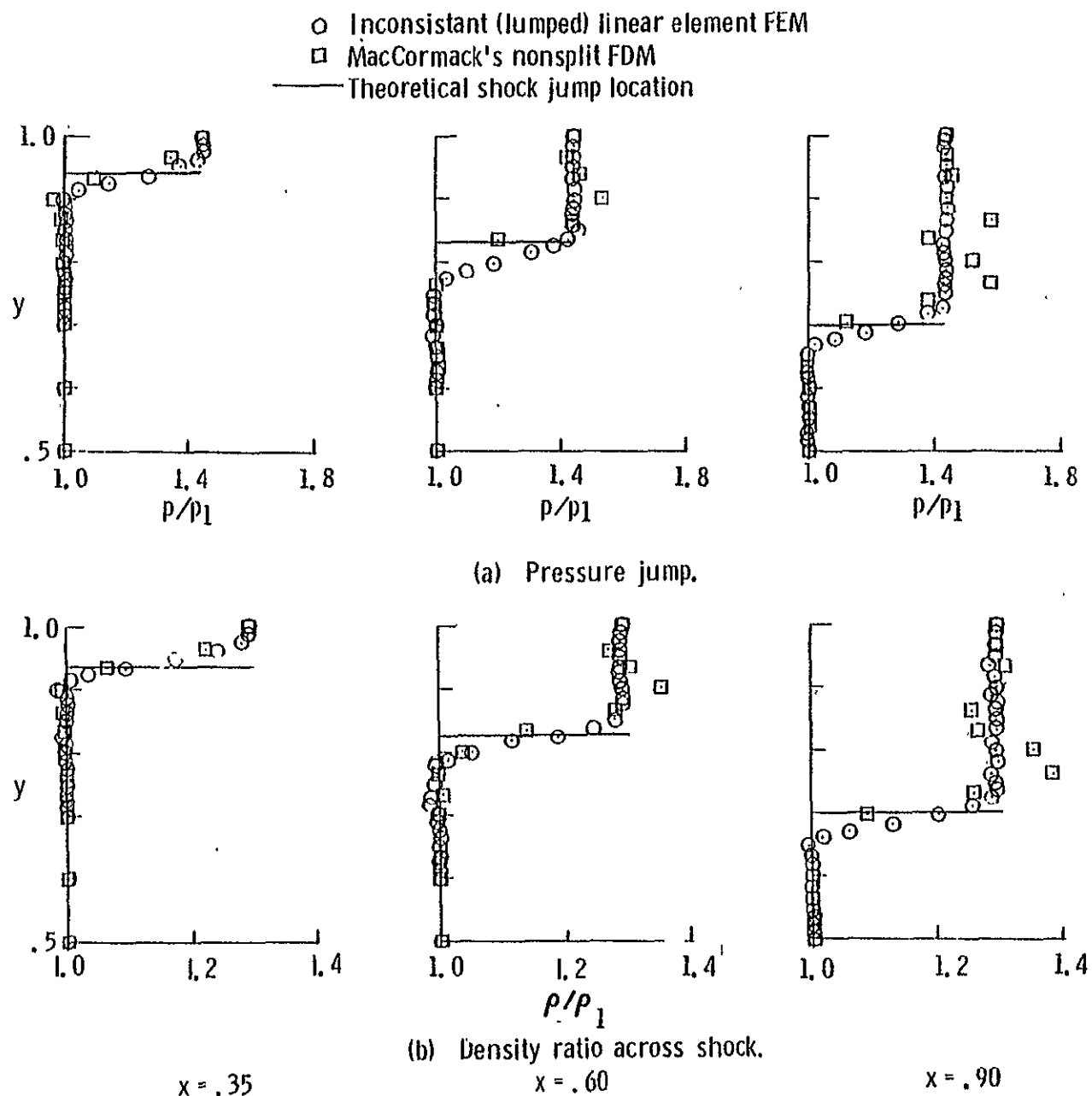
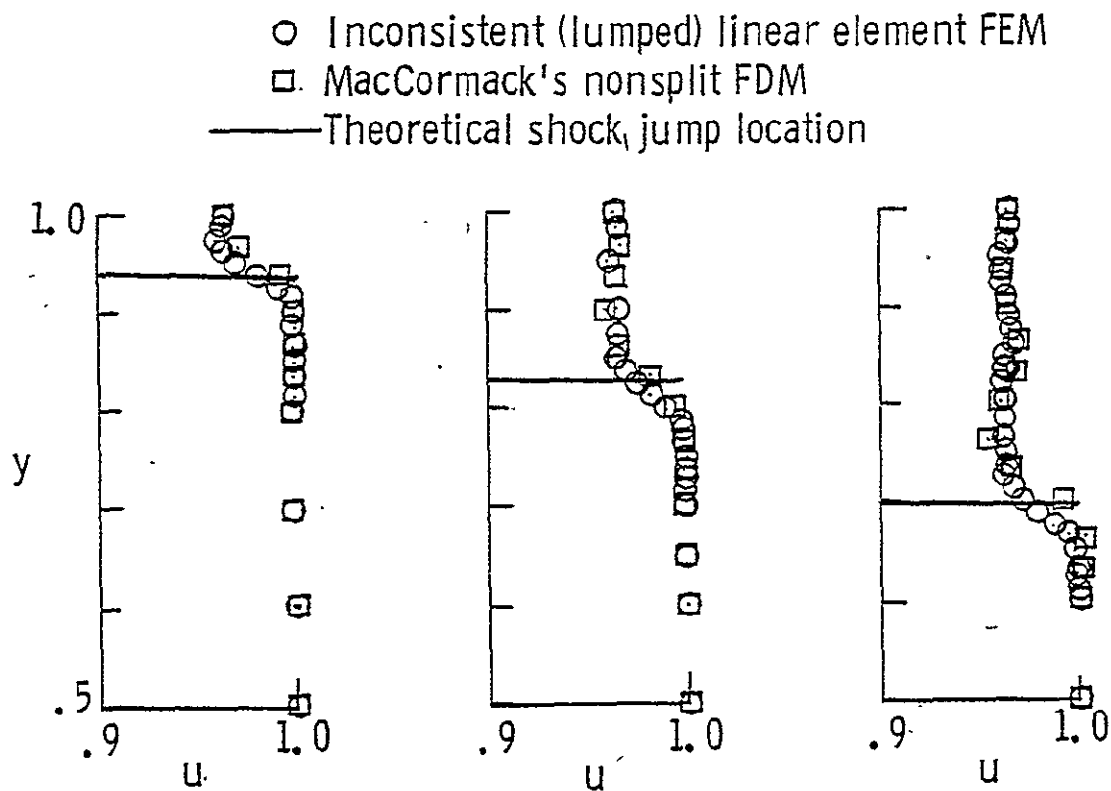
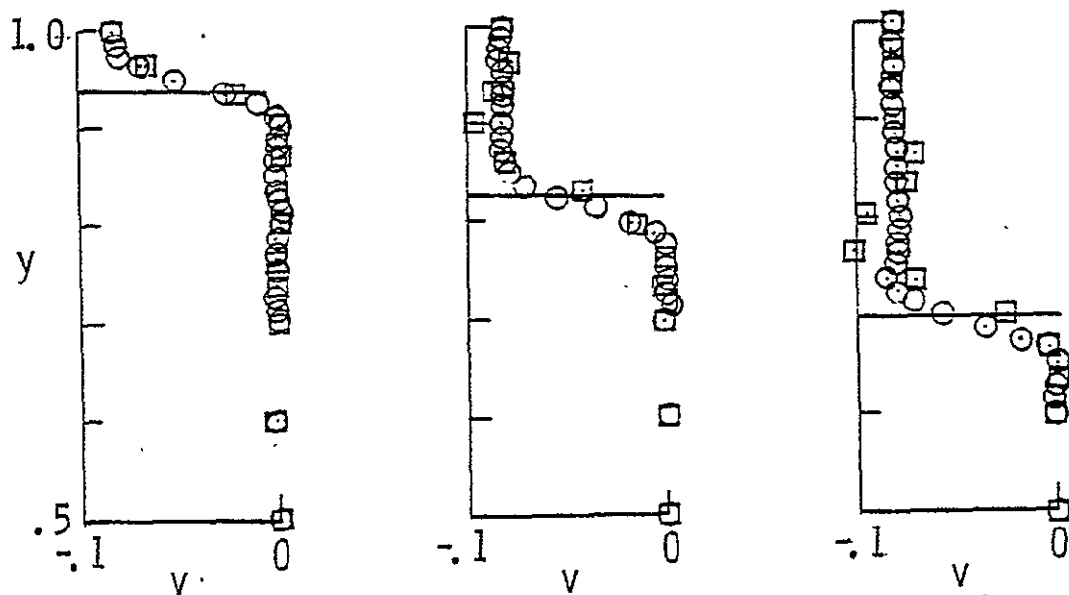


Figure 5. Oblique shock FEM-FDM computational results ($Re = 80,869$).



(c) Streamwise velocity profiles.



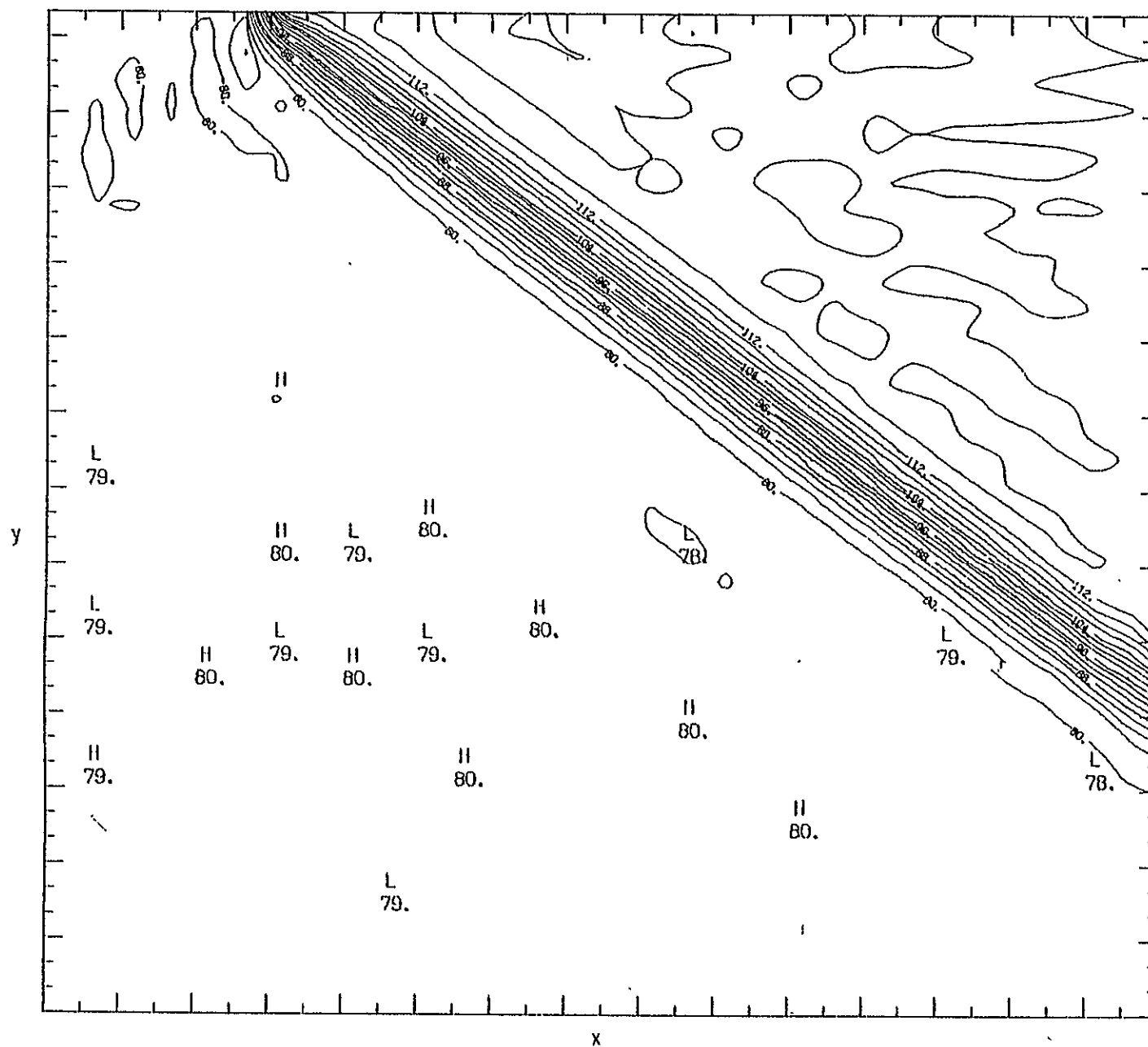
(d) Normal velocity profiles.

$x = .35$

$x = .60$

$x = .90$

Figure 5. Continued.



(e) FEM oblique shock pressure contours.

Figure 5. Concluded.

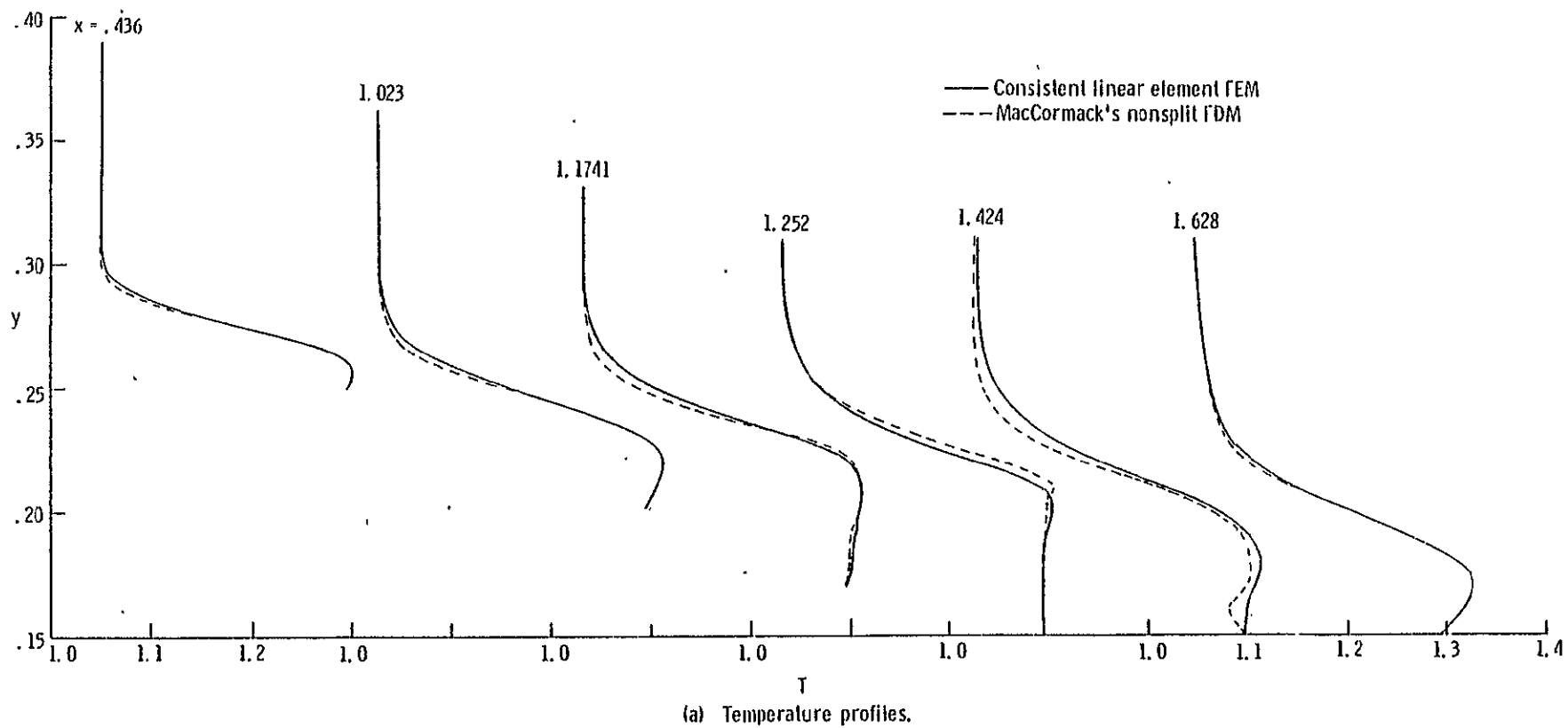
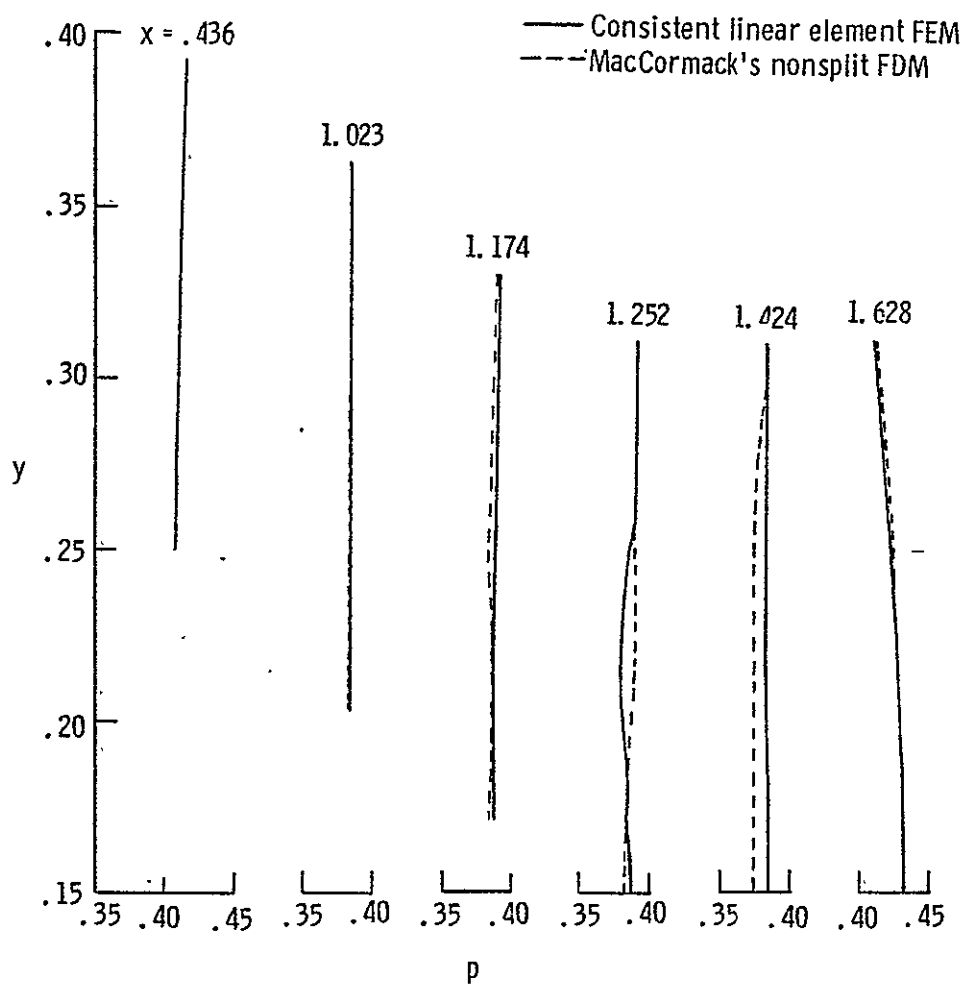
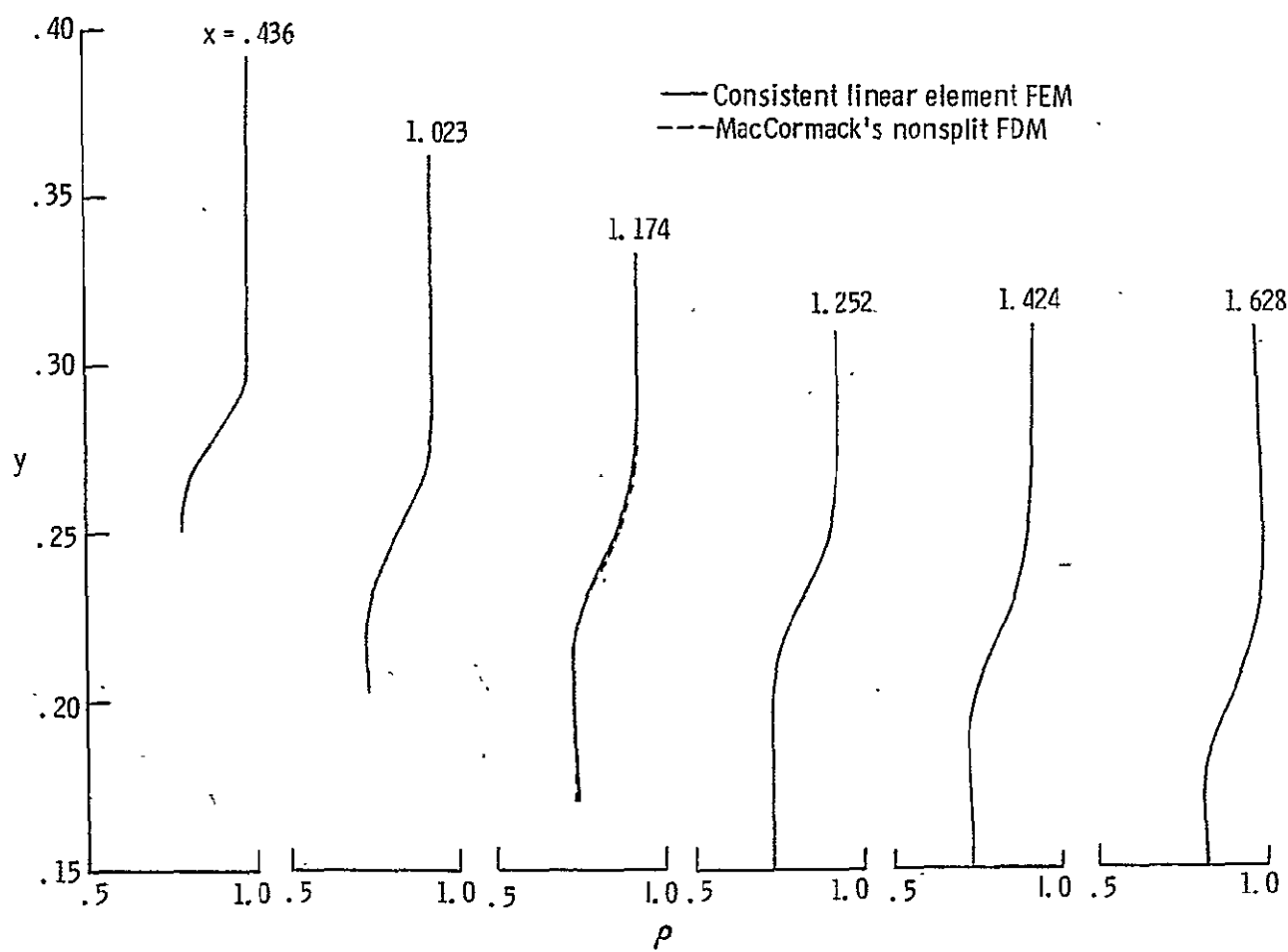


Figure 6. Boattail afterbody FEM-FDM computational results ($Re = 12,365$).



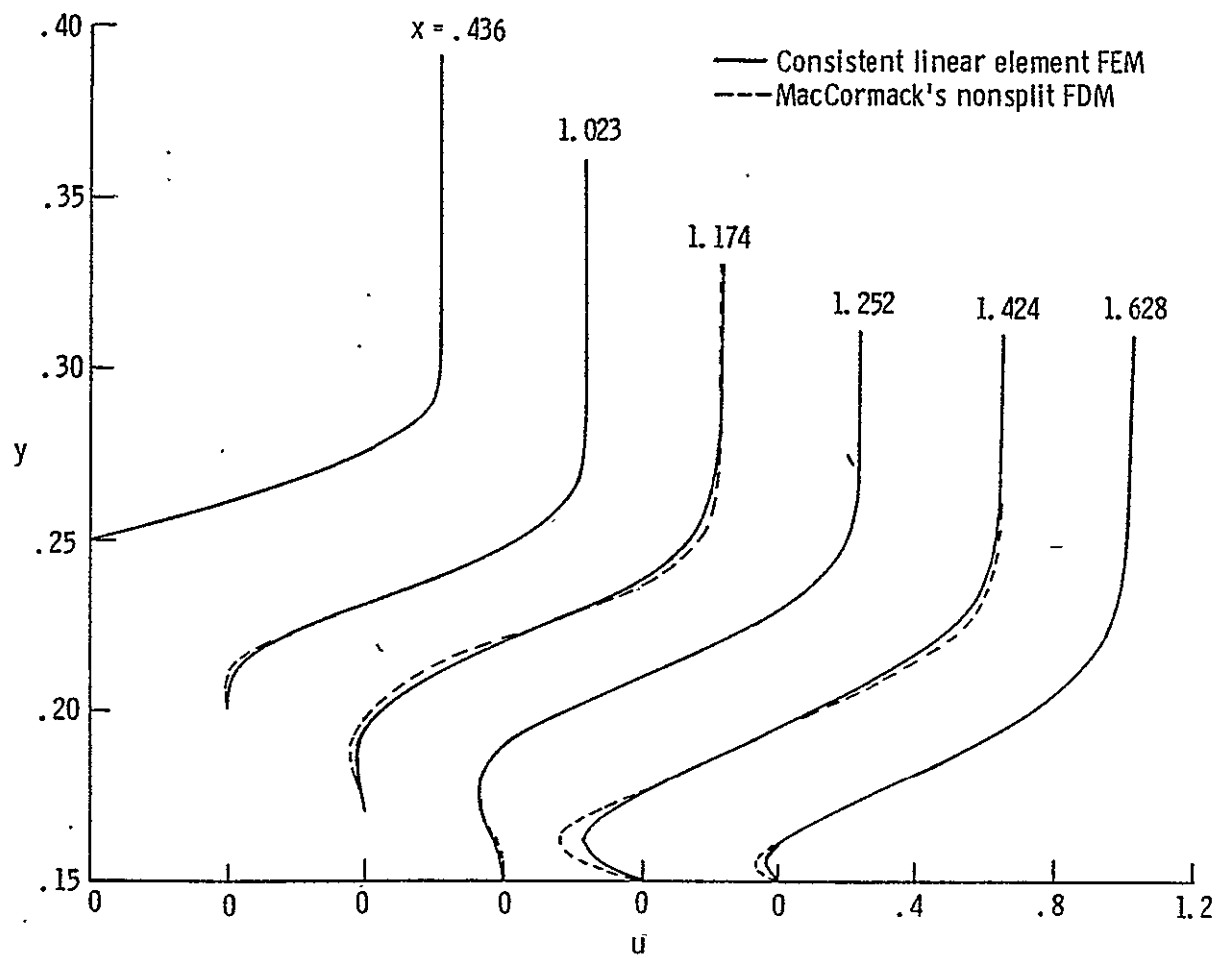
(b) Pressure profiles.

Figure 6. Continued.



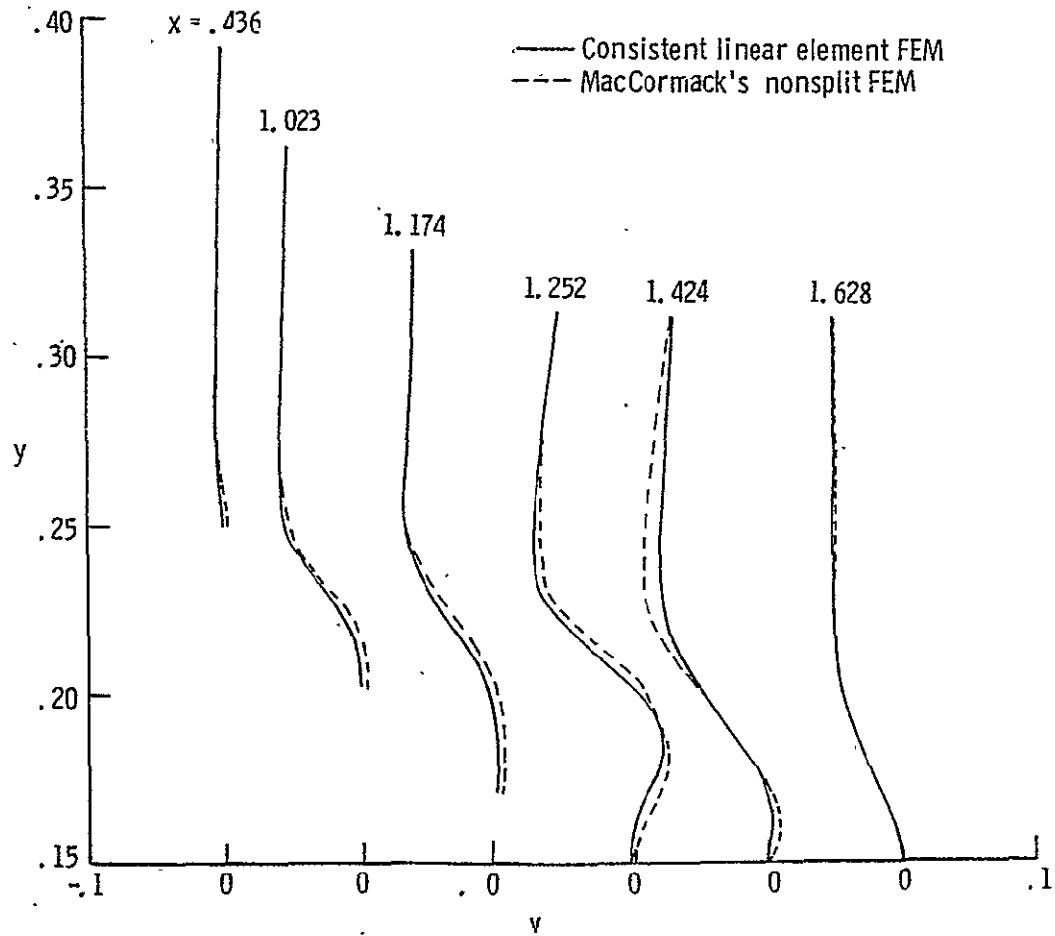
(c) Density profiles.

Figure 6. Continued.



(d) Streamwise velocity profiles.

Figure 6. Continued.



(e) Normal velocity profiles.

Figure 6. Concluded.

APPENDIX I

A SPLIT BAND-CHOLESKY EQUATION-SOLVING STRATEGY FOR FINITE ELEMENT ANALYSIS OF TRANSIENT FIELD PROBLEMS

ABSTRACT

An efficient strategy is outlined for out-of-core solution of the large systems of equations which specify nodal point time derivatives in finite element models of transient flow problems. The positive definiteness, symmetry, and band structure of the finite element mass matrices, as well as the nature of the equation assemblage process, are exploited by the method. Computational results are indicated for systems on the order of several thousand unknowns in size.

INTRODUCTION

A major drawback of finite element as opposed to finite difference models for transient flow problems is that in order to obtain consistent space discretized equations one invariably introduces time derivative coupling of the state variables. For example, space discretized Galerkin models of fluid dynamic interactions governed by the Navier-Stokes equations lead to coupled initial value problems of the form

$$A \frac{d\bar{Q}}{dt} = \bar{F}(\bar{Q}) , \quad t \geq t_0$$

(A-1)

$$\bar{Q}(t_0) = \bar{q}_0$$

In finite element terminology A is the mass matrix of the system (and therefore, symmetric positive definite and time invariant, regardless of physical governing equation characteristics or element type); \bar{Q} is the vector of nodal displacements; and \bar{F} is a nonlinear function of \bar{Q} and boundary constraints.

Preceding page blank

Depending upon the characteristics of the problem and background of the investigator, the inherent implicitness of equations (A-1) has been treated in various ways. Early proponents of implicit time marching schemes such as the Crank-Nicholson Galerkin method (ref. 29), intuitively reasoning matters cannot be worsened by so doing either attack equations (A-1) directly with implicit numerical integration schemes, or else retreat within the Galerkin integral and time discretize implicitly, with resulting marching equation

$$B_n \bar{Q}_{n+1} = \bar{g}_n, \quad n_{\text{past}} \dots \quad (A-2)$$

In such cases the matrices B_n need not be positive definite or even symmetric, which complicates the choice of linear system solver.

On the other hand, a direct attack on the system [eqs. (A-1)] by application of classical explicit methods for numerical integration or ordinary differential equations is hampered by the derivative coupling. Assuming lumping is an unacceptable or unworkable alternative (consistency in the transient is desired and/or higher order elements on nonuniform grids are employed) the tandem matrix inversion required results in what shall be termed a quasi-explicit time marching scheme. Taylor and Davis (ref. 30), possibly motivated by the success of MacCormack's method in numerical fluid dynamics, have experimented with predictor-corrector methods. A typical example is the quasi-explicit modified trapezoidal (lowest order Runge-Kutta scheme)

$$\begin{aligned} A \dot{\bar{Q}}_n &= \bar{f}_n \\ \dot{\bar{Q}}_{n+1}^* &= \bar{Q}_n + \tau \dot{\bar{Q}}_n, \\ \bar{Q}_{n+1} &= \bar{Q}_n + \frac{\tau}{2} (\bar{f}_{n+1}^* + \bar{f}_n), \end{aligned} \quad (A-3)$$

where $\tau = t_{n+1} - t_n$, $\bar{f}_n = f(\bar{Q}_n)$, and $\bar{f}^* = f(\bar{Q}^*)$. A. J. Baker (ref. 31) has achieved some degree of success with quasi-explicit techniques based upon

maximally stable 3-stage one-step self-starting predictor-corrector algorithms (ref. 31).

The relative efficiency of implicit versus quasi-explicit approaches is not decided here. Suffice to say it appears the implicit methods should have an edge, since they are usually absolutely stable, hence have no severe time step limitations. However, for hyperbolic or mixed problems the physics of the flow naturally restricts the time step via the Courant condition (CFL-time-step restriction for explicit finite difference schemes (ref. 22)). This degrades somewhat the advantage of absolute stability usually associated with such schemes. For instance, computational results (ref. 28) indicate the theoretically stable alternating direction implicit (ADI) finite difference method has to be time step restricted to near the explicit CFL limit in order to achieve convergence in the calculation of supersonic compressible free shear flows.

As a consequence, it appears the time step advantage of implicit over quasi-explicit methods may not in all cases be as monumental as at first perceived. The question of how much this advantage can be further offset hinges upon the relative times for assembly of the equations involved, the core storage requirements resulting from program complexity as well as buffers for matrix inversions, and execution speeds for the equation solving. The fact that the mass matrix in equations (A-3) is time invariant and symmetric positive definite enables inversion by the Cholesky method, requiring matrix decomposition only once if auxiliary storage of the triangular components is used, with subsequent front and back solves whenever $\dot{\bar{Q}}_n$ is required. It thus appears the quasi-explicit method, as regards matrix assembly and inversion, could be far more economical, its competitiveness overall then depending largely upon the number of times $\dot{\bar{Q}}_n$ is required per time step.

For the large systems of equations which appear particularly in fluid dynamics applications both classes of methods are further encumbered by the necessity of out-of-core equation-solving strategies. (This may prove to be a greater liability for implicit methods.) The frontal technique of Irons (ref. 25), based on direct Gaussian elimination without pivoting and accomplished with only portions of the matrices assembled at any one time,

has proved an effective solving strategy for symmetric positive definite systems. However, in many cases the matrices of equations (A-2) are unsymmetric; for such Hood (ref. 26) has generalized the frontal technique to allow nonsymmetry and some degree of pivoting. In this section is described an alternate equation-solving choice, the split-Cholesky strategy for banded matrices. This method is characterized by much simpler programming, in comparison, and for large systems should further close the gap between implicit and quasi-explicit integration methods. It is particularly well suited in the circumstance that the triangular decomposition of A is stored on disk, with frontsolves and backsolves whenever $\dot{\bar{Q}}_n$ is needed. For problems governed by the Navier-Stokes equations further economy in storage occurs when boundary conditions allow the same mass matrix for more than one set of dependent variables, such as often happens for the momentum equations in two-dimensional flows.

THE SPLIT-CHOLESKY PHILOSOPHY

The basic idea involved in the split-Cholesky equation-solving strategy is that for a banded matrix the computation can be carried out in pieces, with only a small portion of the matrix residing in core. The essential concepts will be viewed from the position of the analyst familiar with band matrix terminology.

First of all, the band structure inherited by the nonzero portions of the triangular matrices associated with the LU decomposition of a matrix A is identical to the band structure of A . This fact and the nature of the decomposition sequence permit the decomposition to be stored back on top of A as it is performed. Second, if A is symmetric positive definite, then L is the transpose of U ($L = U^T$); hence, only one triangular component must be computed. If U is chosen, only the diagonal and upper triangular portion of the matrix A of equations (A-3) must be assembled. The computation proceeds in stages, with the elements of A to be modified at stage p altered according to the formulas:

$$a_{ik}^{(p)} = a_{ik}^{(p-1)} - R_{pi} R_{pk} ; \quad p = 1, 2, \dots, n ; \quad k \geq i > p$$

(A-4)

$$R_{pp} = a_{pp}^{(p-1)} , \quad R_{pk} = \frac{a_{pk}^{(p-1)}}{R_{pp}} .$$

If A has bandwidth $2m+1$ we see that only rows p through $p+m$ of A need be available in order to accomplish stage p of the decomposition (see diagram 1).

From these considerations it is clear that the Cholesky decomposition of a band matrix can be split into several passes. At each pass a minimum of $p+m$ rows of A must be available in order to perform stage p of the decomposition, with row p the operating row. After this row p is no longer needed; it can be placed on auxiliary storage. Of course, depending upon the size of m and the buffer requirements desired, one would normally decompose stages $p-l$ through p and write $l+1$ rows of U into a single record. The value of l could be related for purposes of convenience to the most logical number of mesh elements to be assembled at one pass, as discussed in the next section. At the same time a record containing several rows of U is completed, the corresponding rows of $L (= U^T)$ which can be made from these rows of U are also assembled, and a record containing several rows of L can also be stored. (As it turns out, portions of the same number of rows of L as there exist available rows of U can be formed.)

MESH CONSIDERATIONS

In order to complete the formulation of the split band-Cholesky strategy it is perhaps helpful to demonstrate the manner in which the assembly of the finite element equations proceeds. The illustration will be accomplished under the assumption of linear trial functions on a triangular mesh. For simplicity the mesh will be obtained from the uniform subdivision of a rectangular region; however, the same ideas hold valid on any mesh whose nodal connections have equivalent topology. (For example, a uniform mesh on a rectangular region can be mapped topologically (and analytically) onto a nonuniform mesh on a nonrectangular region).

Such mappings are commonly used in computational fluid dynamics (ref. 18), and provide a workable device for triangulating a nonregular region in a regular manner so that design of the mesh generator for finite element programs becomes less burdensome.

Consider the triangulated mesh of diagram 2, possessing $NXG (= 8)$ nodes per line of mesh, and leading to mass matrices of semibandwidth $m = NXG$. Normally the finite element assembly proceeds triangle by triangle, with all matrix contributions associated with the unknown (nodal) variables of a triangle to be computed and stored when this triangle is processed. For the split-Cholesky method the assembly is to be completed in several passes, with NL layers of triangles processed at each pass ($NL \geq 2$). Each assembly pass is followed by a decomposition pass, in which the decomposition stage (p) is completed for as many nodal variables x_p , as possible, whose equation is fully summed (completed assembled) during the assembly pass. (At the end of the assembly pass the level of nodes at the front of the pass is only partially summed and thus cannot be processed on this decomposition pass. The preceding level cannot be processed for the same reason, since a decomposition stage at this level must necessarily partially process the nodal equations NXG stages in advance, or in the next level of partially summed nodes.) At the end of the decomposition pass a record containing $NL+1$ rows of U is written disk, together with a record of corresponding rows of $L (= U^T)$. (Some shuffling must be done to account for partial rows of L available but not permitted yet to be stored.) Irregular length records occur on the first and possibly on the last pass.

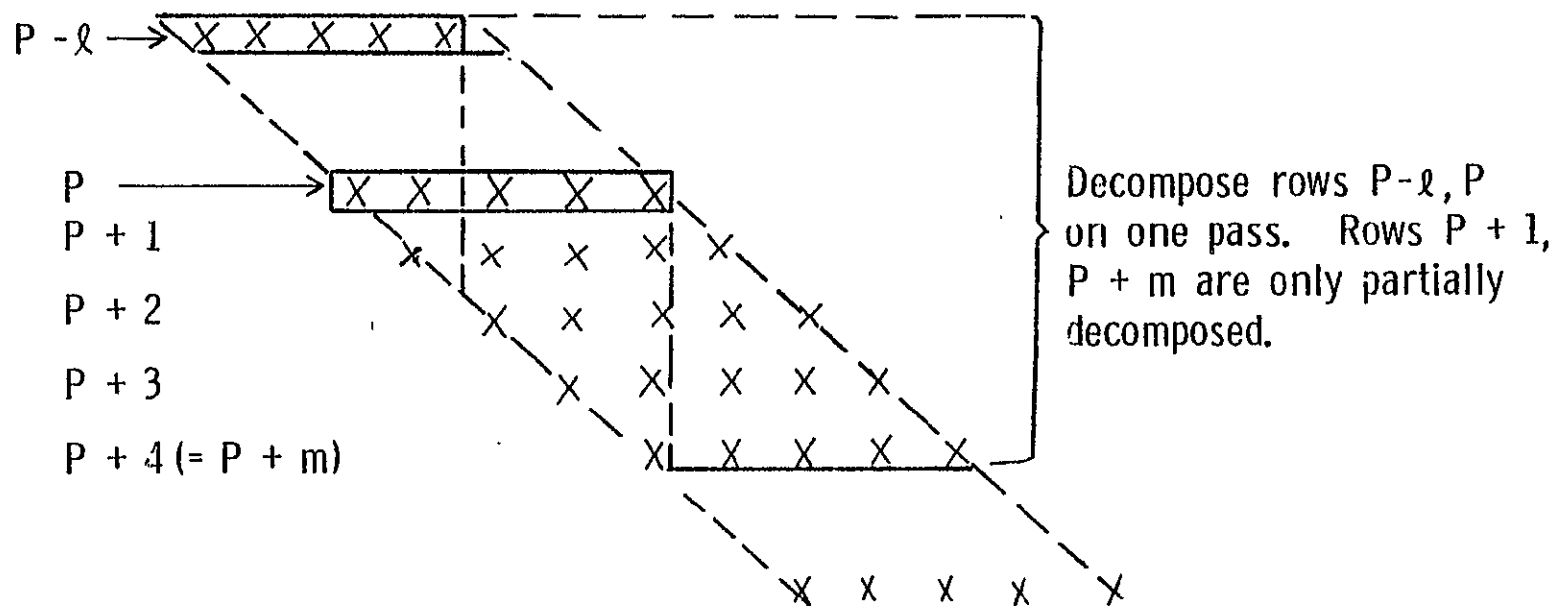


Diagram One. The reduction of a band matrix.

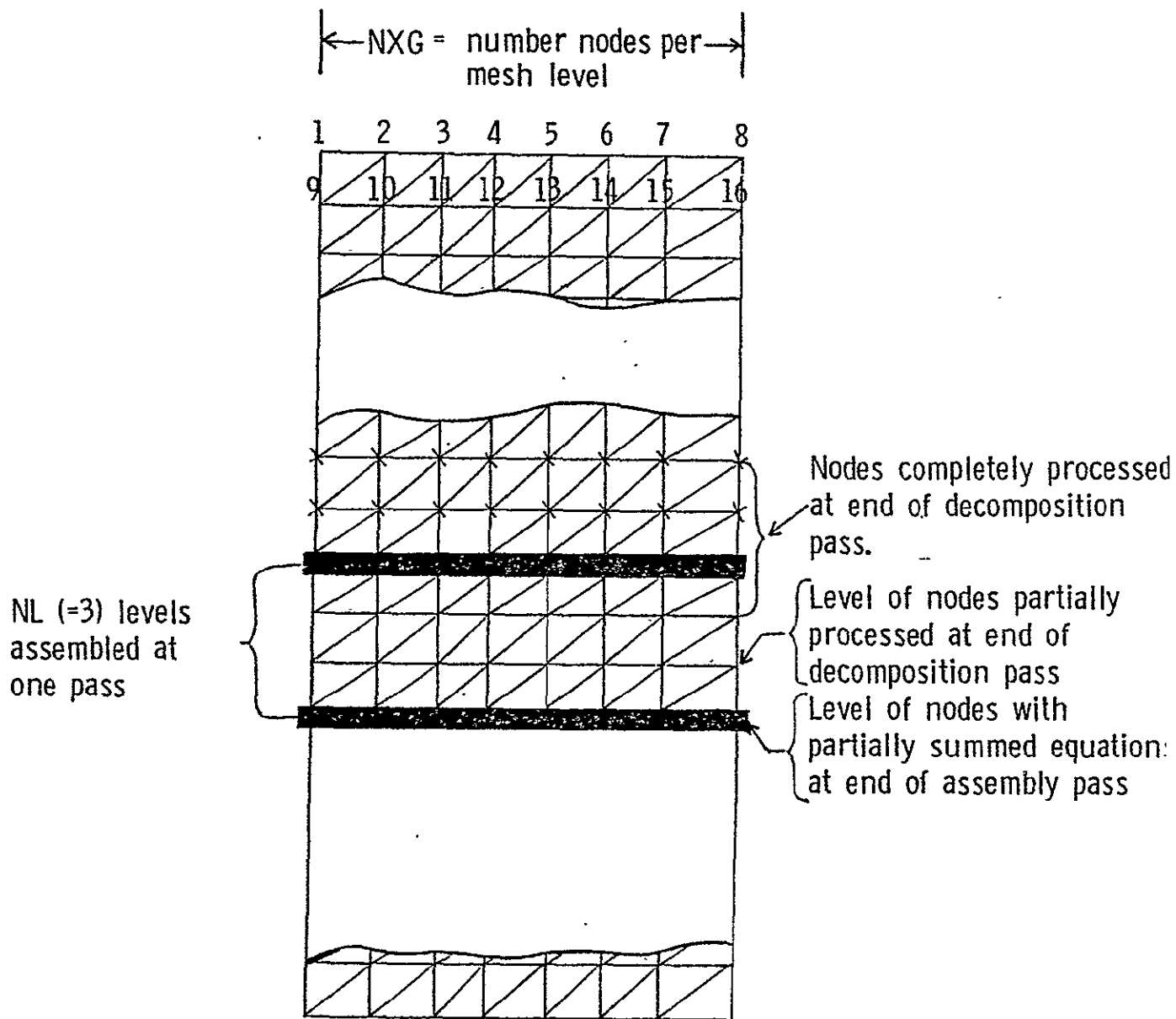


Diagram Two. Mesh Processing Considerations.

REFERENCES

1. Roache, Patrick J., "Recent Developments and Problem Areas in Fluid Dynamics," Lecture Notes in Mathematics, Edited by A. Dold and B. Eckman, pp. 195-256, Springer-Verlag, New York, 1975.
2. Sabir, A. B., "The Nodal Solution Routine for the Large Number of Linear Simultaneous Equations in Finite Element Analysis of Plates and Shells," Finite Elements for Thin Shells and Curved Members, Edited by D. G. Ashwell and R. G. Gallagher, pp. 63-89, John Wiley, New York, 1974.
3. Brashears, M. R.; Chan, S. T. K., et al., "Finite Element Analysis of Transonic Flow," Paper No. L-6, International Conference on Computational Methods in Nonlinear Mechanics, Austin, Texas, September 1974.
4. Baker, A. J. and Popinski, Z., "An Implicit Finite Element Method for the Boundary Layer Equations," *J. Comp. Phys.* 21, (55-84), 1976.
5. Cooke, C. H. and Blanchard, D. K., "A Block Iterative Finite Element Algorithm for Numerical Solution of the Steady-State, Compressible Navier-Stokes Equations," to appear, *Int. J. NME*, 1977.
6. Stephen, G. P., "A Least Squares Finite Element Model for Micro-Meteorological Problems," to appear, *J. Computers and Fluids*, 1978.
7. Habashi, W. G., "The Finite Element Method in Subsonic Aerodynamics," *Proceedings of the Heat Transfer and Fluid Mechanics Institute*, Univ. of Calif. at Davis, June 21-23, 1976 (Stanford University Press).
8. Shen, S. F. and Habashi, W., "Local Linearization of the Finite Element Method and its Applications to Compressible Flows," *Int. J. NME*, Vol. 10, 565-577 (1976).
9. Gartling, David K., "Finite Element Analysis of Viscous Incompressible Fluid Flow," Ph D-Dissertation, TCOM Report 74-8, The University of Texas at Austin, December 1974.
10. Laskaris, T. E., "Finite Element Analysis of Compressible and Incompressible Flow and Heat Transfer Problems," *Phys. of Fluids*, Vol. 18, No. 12, December 1975.
11. Roache, Patrick J., "The LAD, NOS, and Split NOS Methods for the Steady State Navier-Stokes Equations," *Computers and Fluids*, Vol. 3, pp. 179-195, Pergamon Press, 1975.
12. Roache, Patrick J., "The BID Method for the Steady State Navier-Stokes Equations," *Computers and Fluids*, Vol. 3, (305-320), Pergamon Press, 1975.

13. Fix, G. J., "A Mixed Finite Element Scheme for Transonic Flows," ICASE Report No. 76-25, NASA, Langley Research Center, Hampton, VA, 1976.
14. Fix, G. J., "Finite Element Models for Ocean Circulation Problems," SIAM J. Appl. Math., Vol. 29, No. 3, 1975.
15. Fix, G. J., "Effects of Quadrature Errors in Finite Element Approximations of Steady State, Eigenvalue, and Parabolic Problems," Mathematical Foundations of the Finite Element Method with Application to Partial Differential Equations, Academic Press, New York, 1972 (525-556).
16. Fix, G. J. and Gungburger, Max D., "On Least Squares Approximations to Indefinite Problems of Mixed Type," ICASE Report 76-26, NASA, Langley Research Center, Hampton, VA, 1976.
17. Cooke, C. H. and Blanchard, D. K., "Finite Element Computation of a Viscous Compressible Free Shear Flow Governed by the Time Dependent Navier-Stokes Equations," Technical Report, NSG-1098, Dept. of Mathematical and Computing Sciences, Old Dominion University, Norfolk, VA, December 1975.
18. Holst, T. L., "Numerical Solution of Axisymmetric Boattail Flow Fields with Plume Simulators," Paper No. 77-224, AIAA 15th Aerospace Sciences Meeting, Los Angeles, CA, January 24-26, 1977.
19. Hirsh, Richard S., "Numerical Solution of Supersonic Three Dimensional Free Mixing Flows Using the Parabolic-Elliptic Navier-Stokes Equations," NASA TN-D-8195, Langley Research Center, Hampton, VA 1976.
20. Gray, William G. and Pinder, George F., "On the Relationship Between the Finite Element and Finite Difference Methods," Int. J. NME, Vol. 10, 893-923 (1976).
21. Babuska, I. and Aziz, A. K., "On the Angle Condition in the Finite Element Method," SIAM J. Num. Anal., Vol. 13, No. 2, April 1976.
22. Roache, Patrick J., Computational Fluid Dynamics, Hermosa Publishers, Albuquerque, NM, 1972.
23. Bratanow, T.; Ecer, A.; and Kobiske, M., "Finite Element Analysis of Unsteady Incompressible Flow Around an Oscillating Obstacle of Arbitrary Shape, AIAA Journal, Vol. 22, No. 11, November 1973 (1471-1477).
24. Cooke, C. H., "A Split Band-Cholesky Equation Solving Strategy for Finite Element Analysis of Transient Field Problems," to appear, Int. J. NME, 1978.
25. Irons, B. M., "A Frontal Solution Program for Finite Element Analysis," Int. J. NME, Vol. 2, 1970 (5-32).

26. Hood, P., "Frontal Solution Program for Unsymmetric Matrices," Int. J. NME, Vol. 10, 1976 (379-399).
27. Nigro, B. J., "An Investigation of Optimally Stable Numerical Integration Methods with Application to Real Time Simulation," Simulation, Vol. 13, November 1969 (253-264).
28. Rudy, D. H. and Morris, D. J., "Time Asymptotic Solutions of the Navier-Stokes Equations for Free Shear Flows Using an ADI Method," NASA TN D-8217, Hampton, VA, November 1975.
29. Douglas, Jim, Jr. and Dupont, Todd, "Galerkin Methods for Parabolic Equations," SIAM J. Num. Anal., Vol. 7, No. 4, (575-626), December 1970.
30. Taylor, C. and Davis, J., "Tidal and Long Wave Propagation--A Finite Element Approach," Computers and Fluids, Vol. 3, (125-148), Pergamon Press, 1975.
31. Baker, A. J., "Finite Element Solution Algorithm for Viscous-Incompressible Fluid Dynamics," Int. J. NME, Vol. 6, (89-101), 1973.